ORIGINAL PAPER

Claudio Marchesi · Carlos J. Garrido
Marguerite Godard · Joaquín A. Proenza
Fernando Gervilla · Jesús Blanco-Moreno

Petrogenesis of highly depleted peridotites and gabbroic rocks from the Mayarí-Baracoa Ophiolitic Belt (eastern Cuba)

Abstract The Moa-Baracoa and Mayarí-Cristal massifs (eastern Cuba) are two ophiolitic complexes mainly constituted by harzburgite tectonites and minor dunites, cut by gabbroic dykes. The Moa-Baracoa massif exhibits a well developed Moho transition zone and an incomplete crustal section made up of layered gabbros and tectonically emplaced pillow basalts. A plutonic crustal section is absent in the Mayarí-Cristal massif and mantle tectonites are in tectonic contact with arc-related volcanic rocks. Mantle peridotites are very refractory in terms of modal composition, whole rock major element and HREE contents implying that Moa-Baracoa and Mayarí-Cristal harzburgites are residues after high degrees (20–30%) of partial melting. The relative enrichment of Th, Nb, Ta and LREE in peridotites is due to re-equilibration of melting residues with percolating melts. Peridotites lost on average 6 wt% of relative MgO by intense seafloor weathering. REE contents and Mg# of melts in equilibrium with cumulate gabbros from the Moho transition zone and crustal section of the Moa-Baracoa massif coincide with those of the spatially-related pillow basalts. On the other hand, no geochemical relation has been inferred between melt in equilibrium with Mayarí-Cristal segregate and the spatially-related arc volcanics. Our results indicate that the Mayarí-Baracoa Ophiolitic Belt formed at an original back-arc spreading centre. The Moa-Baracoa massif represents a portion of MORB-like lithosphere located nearby a back-arc mid-ocean spreading ridge, and the Mayarí-Cristal massif represents a piece of transitional (MORB to IAT) mantle located closer to the paleo-volcanic arc than Moa-Baracoa.

C. Marchesi · F. Gervilla
Instituto Andaluz de Ciencias de la Tierra, Facultad de Ciencias,
Universidad de Granada - CSIC, Granada, Spain

C. J. Garrido · C. Marchesi (✉) · F. Gervilla
Departamento de Mineralogía y Petrología, Facultad de Ciencias,
Universidad de Granada, Avenida Fuentenueva s/n,
18002 Granada, Spain
E-mail: claudio@ugr.es

M. Godard
Laboratoire de Tectonophysique, ISTEEM,
Université Montpellier II, Montpellier, France

J. A. Proenza
Departament de Cristal·lografia, Mineralogia i Dipòsits Minerals,
Facultat de Geologia, Universitat de Barcelona, Barcelona, Spain

J. Blanco-Moreno
Instituto Superior Minero-Metalúrgico de Moa,
Las Coloradas, s/n, Moa, Holguín, Cuba

Introduction

In the Caribbean Triassic to Recent evolution two main tectonic phases can be identified. First, the Proto-Caribbean oceanic basin opened as a result of drift between North America and Gondwana; afterwards a collisional phase led to the development of several volcanic arc systems and the consumption of Proto-Caribbean (Atlantic) and/or Caribbean (Pacific-Farallon) crust (e.g. Meschede and Frisch 1998; Iturralde-Vinent 1998 and references therein). As a result of these collisional events, several ophiolitic massifs were emplaced in Cuba along the so-called "Northern Cuban Ophiolite Belt" constituted by dismembered mafic–ultramafic bodies cropping out along an east–west trend in northern Cuba (inset in Fig. 1a). Cuban ophiolites are interpreted as oceanic lithosphere slabs either from a Proto-Caribbean back-arc basin related to subduction of the Pacific plate (e.g. Iturralde-Vinent 1998), remnants of the subducting Proto-Caribbean oceanic lithosphere emplaced onto the Pacific paleomargin, or forearc lithosphere built on the Pacific paleomargin (e.g. Pindell and Barrett 1990; Pindell 1994).

In spite of their importance in the context of the geodynamic evolution of the Caribbean realm, the structure, petrology and geochemistry of Cuban ophiolites are poorly documented. Volcanics spatially-related

Fig. 1 a Geological map of the Mayarí-Baracoa Ophiolitic Belt with location of studied samples (*circles*). *1* Middle Eocene-Quaternary sediments, *2* Tertiary volcanic rocks, *3* Upper Campanian–Lower Danian sediments, *4* Ophiolitic melange (La Picota), *5* Cretaceous volcanic rocks, *6* Diorites, *7* Melange La Corea, *8* Diabases and microgabbros, *9* Gabbros, *10* Serpentinized Peridotites, *11* Foliation, *12* Faults, *13* Sample locations. *Inset* Geographic location of massifs constituting the Northern Cuban Ophiolite Belt; *black box* indicates the Mayarí-Baracoa Ophiolitic Belt. **b** Schematic lithostratigraphic columns of Mayarí-Cristal and Moa-Baracoa massifs
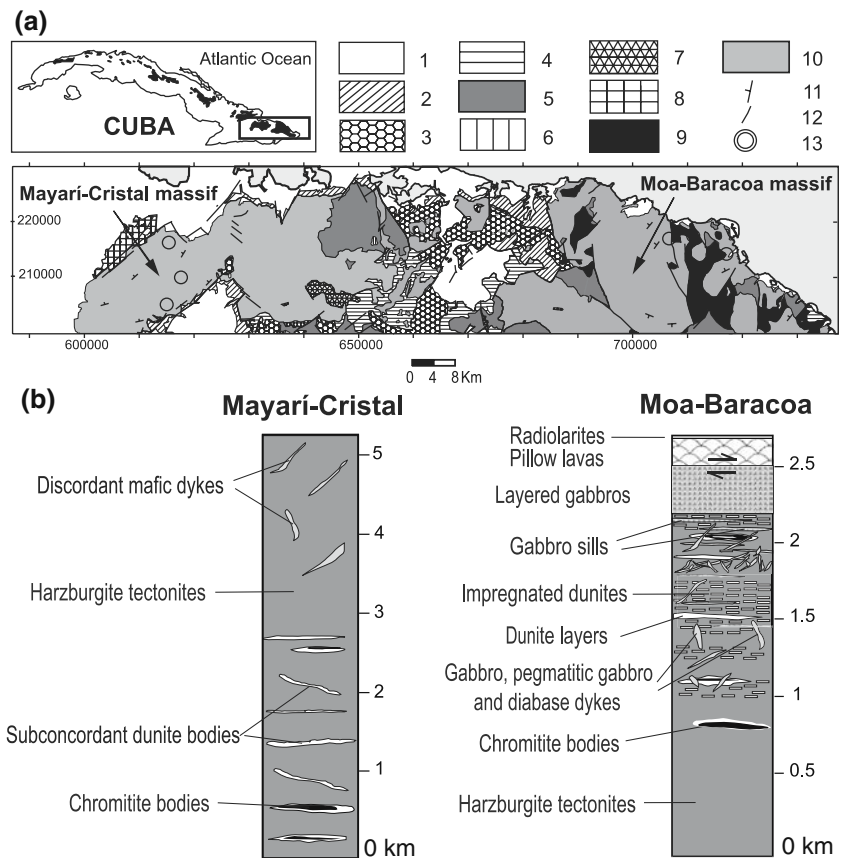
with ophiolites have a subduction-related character (Kerr et al. 1999; García-Casco et al. 2003; Proenza et al. 2006). Geochemical data on residual peridotites and ophiolite gabbros are, however, needed to clarify key geodynamic issues such as the Pacific versus Atlantic (Proto-Caribbean) provenance of the oceanic lithosphere, the supra-subduction, back-arc and/or mid-ocean spreading-ridge nature of these ophiolites, and the genetic link between ophiolite plutonics and arc volcanics. In this paper we present new petrological and geochemical data on a representative sample set from the Mayarí-Baracoa Ophiolitic Belt (MBOB), the easternmost massifs of the Northern Cuban Ophiolite Belt. We show that the MBOB is constituted by highly depleted peridotites and cumulate gabbroic rocks formed at a back-arc spreading centre. The eastern region of the MBOB (Moa-Baracoa massif) represents a piece of lithosphere originally located close to the spreading centre, and the western region (Mayarí-Cristal massif) represents a portion of transitional (MORB-IAT) lithospheric mantle originally situated closer to the paleo-volcanic arc than Moa-Baracoa.

Geological setting

The MBOB is located in the easternmost part of the Northern Cuban Ophiolite Belt, a set of strongly faulted ultramafic, plutonic, volcanic and sedimentary melange complexes outcropping in northern Cuba (inset in Fig. 1a). This Ophiolitic Belt is part of the Cuban foldbelt, an orogenic unit made up of deformed and metamorphosed tectonic nappes accreted in the late Cretaceous-late Eocene during the northward collision of the western Caribbean volcanic arc with the Bahamas continental platform (Iturralde-Vinent 1994, 1996).

The plate tectonic evolution of the Caribbean is complex and investigators have not yet come to a consensus on a geodynamic model capable of integrating the geologic observations available in this region (e.g. Iturralde-Vinent 1994). The Proto-Caribbean oceanic crust was formed in late Triassic-early Cretaceous during continental rifting and ensuing opening of an oceanic basin between the North and South America plates (Pindell 1994). In the Cretaceous, several volcanic arcs were produced along a subduction zone located between the Proto-Caribbean and the Pacific Caribbean oceanic plates. The number of volcanic arcs formed during this phase and the relative polarity of the subduction zones are open to debate (Iturralde-Vinent 1998). Some authors (e.g. Iturralde-Vinent 1998; Kerr et al. 1999) propose that several volcanic arcs were built upon the Proto-Caribbean oceanic crust by underthrusting of the Pacific Caribbean plate beneath the Proto-Caribbean. Other authors (Pindell and Barrett 1990; Pindell 1994) claim that these arcs were accreted on the Pacific Caribbean plate during subduction of the Proto-Caribbean plate. These two different models have led to

differing paleogeographic reconstructions of the Cuban paleo-arcs and interpretations of the origin of the Cuban ophiolite belt (e.g. Iturralde-Vinent 1994 and references therein).

Based on the geochemistry of Cretaceous volcanic rocks in Cuba, Kerr et al. (1999) proposed the existence of two pre-Albian volcanic arcs: one composed of boninites and the other of island arc tholeiites that subsequently evolved to a calcalkaline–alkaline Albian–Campanian arc. During the Paleogene a new volcanic arc system developed in the Caribbean realm. In Cuba it is essentially represented by the volcano-sedimentary rocks cropping out in the Sierra Maestra range (Cazañas et al. 1998; Kysar Mattietti 2001). After the Paleogene the subduction activity shifted to the eastern Caribbean zone due to strike slip fault systems (e.g. Oriente fault) and it is nowadays located in the Lesser Antilles arc.

Mayarí-Baracoa Ophiolitic Belt: field relations and petrography

The MBOB is a pseudotabular, strongly faulted, mafic-ultramafic massif occurring in eastern Cuba (Fig. 1a). The MBOB is ca. 170 km long, 10–30 km wide and 3.5 km thick on average. The MBOB comprises two different massifs (Proenza et al. 1999a, b): the Moa-Baracoa massif to the east and the Mayarí-Cristal massif to the west (Fig. 1a). The MBOB is thrusted over volcanic and sedimentary rocks of late Cretaceous age (Fig. 1a). Moa-Baracoa peridotites and gabbroic rocks are in tectonic contact with Morel volcanics of Turonian or early Coniacian age (Iturralde-Vinent et al. 2006), whereas the easternmost part of the Mayarí-Cristal massif is thrusted over the Téneme volcanics which are partially isochronous with the Morel volcanism (Iturralde-Vinent et al. 2006). Field evidence indicates that the final emplacement of the MBOB occurred during the Maastrichtian (Cobiella-Reguera 2002; Iturralde-Vinent 2003). Upward, the MBOB is occasionally in contact with the undeformed rocks of Paleogene arc or it is covered by post-Upper Eocene sandstones and siltstones (Iturralde-Vinent 1996).

The Moa-Baracoa massif

The Moa-Baracoa massif is made up of a section (> 2.2 km thick) of mantle tectonite harzburgite with subordinate dunite, and a Moho transition zone (MTZ) overlain by layered gabbros of the lower oceanic crust (ca. 500 m thick). All outcropping sections of the Moa-Baracoa massif lack exposures of isotropic gabbros and diabase sheeted-dyke complexes archetypical of the conventional ophiolite sequence (Nicolas 1989 and references therein). This is most likely due to tectonic omission as in some localities layered gabbros are directly overlain by tectonically discordant pillow lavas and radiolarites (30–40 m t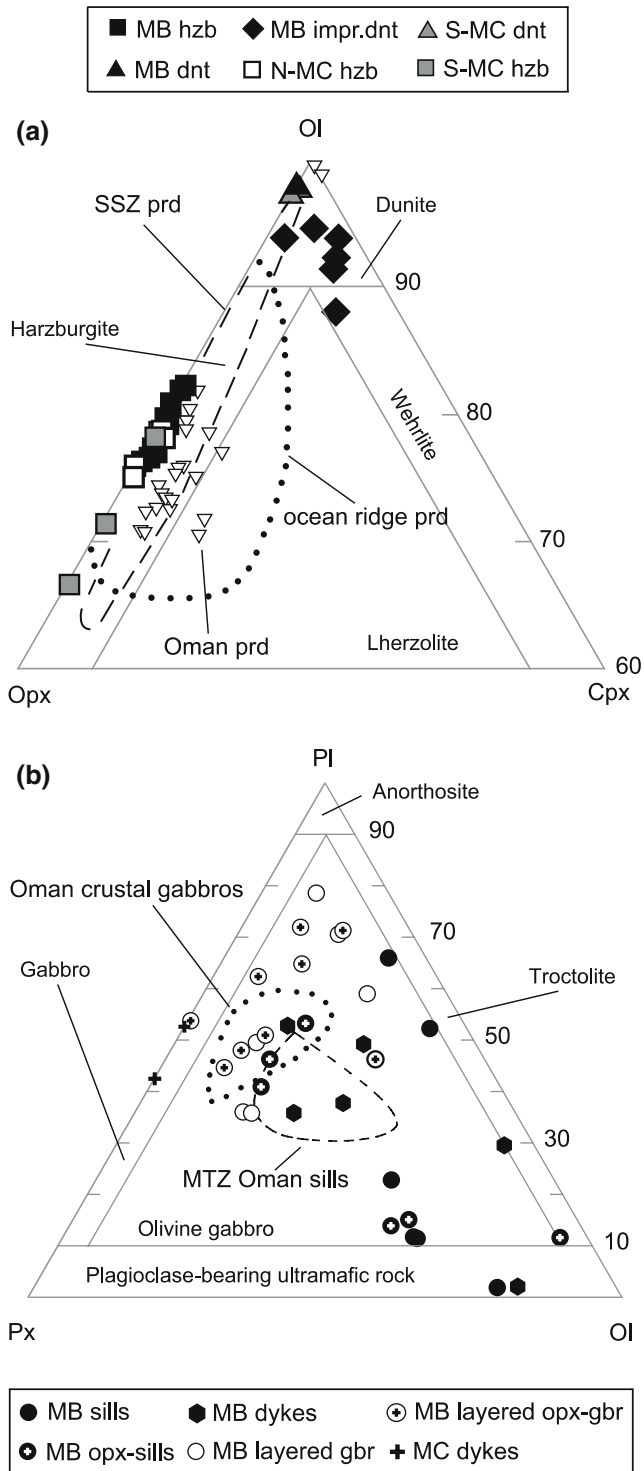hick). In our field studies we did not find continuous sections from tectonite to layered gabbro owing to poor exposure in the tropical forest and/or pervasive faulting. The field description below corresponds to observations in good exposures of different sections of the massif cropping out in the localities of Quemado del Negro (crustal layered gabbros), Mercedita Mine (MTZ sills and dykes), Cayo Guam and Yamaniguey (harzburgite tectonites, MTZ dunites, gabbro sills and dykes). Despite poor exposure, our regional mapping indicates that the presence of a MTZ is a regular feature at the scale of the Moa-Baracoa massif, and it points to a lithological section as portrait in Fig. 1b.

The Moa-Baracoa mantle section displays a penetrative foliation generally NNW dipping. Harzburgite tectonite is locally cut by gabbro dykes and minor pegmatitic gabbro, diabase, pyroxenite, troctolite and wehrlite, which are increasingly abundant near the MTZ (Proenza et al. 1999a).

We calculated the primary mode of peridotites (Fig. 2a) by computer-assisted point counting on large thin sections following procedures of Dick et al. (1984) for highly altered abyssal peridotites. Point-counting and petrographic observations show that MBOB harzburgites lack clinopyroxene (cpx), except for tiny cpx exolutions in orthopyroxene (opx). The absence of cpx was confirmed by careful checking under binocular microscope of different mineral separate fractions obtained on large sample amounts.

Moa-Baracoa harzburgites display the common porphyroclastic texture of ophiolite tectonites characterized by 1–4 mm olivine (ol) and opx up to 1.5 cm long. The matrix consists of 200–500 μm polygonal ol and opx and minor xenomorphic Cr-rich spinel.

The MTZ is characterized by harzburgite and sub-concordant dunite showing sharp contacts with harzburgite. In terms of their cpx modal content, we differentiate two types of dunite: *dunite (sensu stricto)* and cpx-pl (plagioclase) rich dunite that we will refer hereafter to as *"impregnated"* dunite (Fig. 2a). Dunites show equigranular ($\sim$ 1 mm) textures made up of weakly deformed ol, very rare opx and anhedral to euhedral spinel. Impregnated dunites occur within MTZ dunite as centimetric cpx- and pl-rich patches that modally correspond to plagioclase-dunites and plagioclase-wehrlites (Fig. 2a). Plagioclase (totally altered to phyllosilicates) is texturally associated with subhedral 2–3 mm cpx and fine grained spinel forming interstitial clusters between ol. Spinel also occurs in euhedral grains intergranular between ol and opx. In terms of field occurrence, Moa-Baracoa impregnated dunites are similar to impregnated dunites described in the MTZ of the Oman ophiolite (Godard et al. 2000; Jousselin and Nicolas 2000; Koga et al. 2001), although such dunites are also common in some orogenic and abyssal peridotite exposures (Bodinier and Godard 2003). Such impregnated dunites testify "refertilization" processes due to pervasive interaction of the mantle with basaltic melts (e.g. Hellebrand et al. 2002; Bodinier and Godard 2003).

crustal layered gabbros, to troctolites to plagioclase peridotites (Fig. 2b). This modal variability mainly reflects high ol contents in samples with diffuse transitions to enclosing dunites at the hand-specimen scale. Secondary magnetite, as product of ol serpentinization, is the only oxide present.

Olivine gabbro and minor troctolite and plagioclase-bearing ultramafic dykes (Fig. 2b) have been observed mainly in the MTZ. Ol gabbro dykes display variable grain size (up to several decimetres in pegmatitic samples) and degrees of alteration. Titanite has occasionally been observed as alteration product.

Crustal layered gabbros are composed of ol gabbros and minor gabbros that are in part opx-bearing (Fig. 2b). The great variability of modal plagioclase is due to a sampling bias related to uneven plagioclase/mafic mineral ratios in our samples. Modal layering, defined by variations of the mafic mineral/plagioclase ratio, is oriented N30°E dipping 30–50°NW and is broadly parallel to the regional harzburgite tectonite foliation. The contact between the different mafic rocks is transitional. Ol is dispersed between dominant plagioclase and cpx, the latter generally interstitial between plagioclase laths. On the basis of textural observations, plagioclase began to crystallize prior to cpx in these gabbroic rocks.

The Mayarí-Cristal massif

The Mayarí-Cristal massif is essentially a peridotite massif (> 5 km thick) made up of harzburgite tectonite hosting minor subconcordant dunite layers and subordinate discordant microgabbro dykes (Fig. 1b). Detailed mapping shows the absence of a MTZ and plutonic crustal section. Previous investigators have described the existence of a sheeted-dyke complex in the northwestern part of the massif. Our reconnaissance studies indicate that this complex is a subvolcanic formation made up of massive microgabbros in tectonic contact with harzburgite tectonites (Fig. 1a). The link between this unit and the Mayarí-Cristal tectonites is uncertain.

Another particularity of the MTZ is the presence of gabbro sills (several meters thick) showing misty gradations to the enclosing MTZ dunites due to variation of the plagioclase/mafic mineral (cpx + ol) modal ratio. Modal abundances of gabbroic rocks were determined by mass balance between whole rock and single mineral compositions. Gabbro sills show a wide modal variation ranging from ol (orthopyroxene) gabbros similar to

The Mayarí-Cristal harzburgites display porphyroclastic texture. They are cpx-poor and generally have higher opx/ol ratios than Moa-Baracoa harzburgites (Fig. 2a). In terms of field occurrence, we differentiate two domains in the western part of the Mayarí-Cristal massif:

1. A northern domain mainly constituted by harzburgite tectonites with a NE–SW oriented foliation dipping 25–55° NW. Dunites are scarce in this region. This domain is characterized by the presence of swarms of microgabbros discordant to the enclosing harzburgite tectonites. Microgabbro dykes are gabbros and hornblende-bearing gabbros (Fig. 2b), 5 cm to 10 m thick, with a maximum grain size of 1 mm decreasing toward the harzburgite wall-rocks. This indicates that, conversely to Moa-Baracoa gabbros, Mayarí-Cristal microgabbro dykes intruded in a relatively cold oceanic mantle lithosphere. Because of the lack of a plutonic crustal section and a MTZ, along with the occurrence of microgabbros intruding tectonites, the northern domain of the Mayarí region resembles the ultramafic exposures described at slow-spreading oceanic ridges, as for the mid-Atlantic ridge (Bonatti et al. 1971; Cannat et al. 1997) and the Mariana Trough (Ohara et al. 2002).

2. A southern domain mainly composed of harzburgite tectonites with a NE–SW oriented foliation dipping 25–60°NW. In this domain highly serpentinized dunites are widespread and generally occur as irregular patches or subconcordant layers (< 1 m thick) within harzburgite tectonites. We have also observed thicker dunite bodies (1–3 m) hosting chromitite lenses. As in Moa-Baracoa, the contact between dunites and harzburgite tectonites is sharp. In most of the harzburgites the only phase which is not completely altered is the Cr-rich spinel.

Secondary alteration of MBOB peridotites

A general feature of MBOB peridotites is that they are highly altered. The main alteration type is due to serpentinization. Available stable isotope data indicate that serpentinization occurred by ingression of seawater during the oceanic stage of MBOB peridotites (Proenza et al. 2003). Moa-Baracoa peridotites show variable degrees of serpentinization ranging from 60 to 90% in most samples, and serpentinization in Mayarí-Cristal peridotites is pervasive especially in those from the southern domain. The imprints of serpentinite alteration on MBOB peridotites are the transformation of ol to lizardite–magnetite assemblages displaying mesh and non-pseudomorphic textures, and the alteration of opx to pseudomorphic (bastite) and non-pseudomorphic serpentine and, locally, to talc. Conversely, spinel is virtually fresh in all samples and only exhibits thin rims of ferrichromite. In addition to serpentine-group minerals, clay minerals were also detected by X-ray diffraction in most of the samples.

Finally, MBOB peridotites usually display a thick reddish crust of sub-aerial iron oxide and clay minerals owing to intense tropical weathering, and minor carbonate veins. The studied samples lack pervasive talc alteration.

Sampling and analytical methods

For this study we have selected 61 samples that are representative of the main lithological types of the MBOB. Peridotite samples ($n = 16$) from Moa-Baracoa are nine harzburgites, one dunite and six impregnated dunites (Table 1). Gabbroic samples from Moa-Baracoa ($n = 33$) comprise (Table 2): different types of gabbros from the crustal section ($n = 15$); sills of ol gabbros ($n = 10$), troctolite ($n = 1$) and werhlite ($n = 1$) in the MTZ; and intrusive dykes of ol gabbro ($n = 4$), troctolite ($n = 1$) and werhlite ($n = 1$) in the MTZ. Samples from the northern Mayarí-Cristal massif encompass four harzburgites and two gabbroic dykes (Tables 1, 2). Samples of dunite are not available because of the virtual absence of this lithotype in the northern Mayarí-Cristal massif. Peridotites from the southern Mayarí-Cristal massif are four harzburgites and two subconcordant dunites (Table 1).

Mineral compositions were obtained in rock thin sections by electron microprobe using a WDS-CAMECA SX 50 instrument at the Serveis Cientificotècnics of the Universitat de Barcelona (Spain). Excitation voltage was 20 kV and beam current 15 nA, except for analyses of Cr-rich spinel for which a current of 20 nA was preferred. Most elements were measured with a counting time of 10 s, except for Ni, V and Zn (30 s).

For whole rock analyses, veins and Fe oxide/clay crust were carefully removed before sample crushing. Sample powders were made by crushing and powdering large amounts of each sample (usually > 3 kg) in an agate ring mill. Whole rock major and minor transition elements (Ni, V and Cr) were analysed by XRF at the Universidad del País Vasco (Spain) and at the Centro de Instrumentación Científica of the Universidad de Granada (Spain) in a PHILIPS PW1404/10 instrument using standard sample preparation and analytical procedures.

Whole rock trace elements (REE, Cs, Rb, Th, U, Nb, Ta, Sr, Zr, Hf, Li and Co) were analysed by a VG-PQ2 Turbo + Inductively Coupled Plasma-Mass Spectrometer (ICP-MS) at ISTEEM (Université Montpellier II, Montpellier, France). Whole rock trace element data of MBOB peridotites and gabbros are reported in Tables 1 and 2, respectively. REE, Cs, Rb, Th, U, Sr, Zr, Hf, Li and Co concentrations were determined by external calibration following the HF/HClO$_4$ dissolution and analytical procedure described in detail by Ionov et al. (1992). To avoid memory effects due to the intake of concentrated Nb–Ta solutions in the instrument, Nb

Table 1 Whole rock major and trace element data of studied peridotites from the Mayarí-Baracoa Ophiolitic Belt

Location   Moa-Baracoa massif

Rocktype	Harzburgite									Dunite	Impregnated dunite	
Sample	CG 3	CG 5	CG 6	CG 7	CG 10	CG 13	CG 14	YM 14	YM 16	CG 16	CG 1	CG 2
SiO_2(wt%)	38.55	39.23	41.89	36.66	38.02	38.23	37.45	38.19	39.11	36.81	38.66	38.29
TiO_2	0.006	0.008	0.007	0.005	0.005	0.016	0.006	0.004	0.002	0.005	0.05	0.06
Al_2O_3	0.42	0.95	0.85	0.70	0.86	0.70	0.57	0.34	0.33	0.52	3.09	2.38
Fe_2O_3	8.01	7.60	7.72	7.69	8.05	8.29	7.79	7.56	7.56	7.68	9.50	9.85
MnO	0.11	0.12	0.13	0.11	0.11	0.11	0.11	0.11	0.11	0.11	0.13	0.14
MgO	38.01	36.81	37.63	38.26	35.47	40.62	38.24	39.09	40.34	38.65	35.69	36.31
CaO	0.35	0.32	0.48	0.32	0.05	*0.28*	bdl	0.17	0.57	0.34	0.80	0.67
Na_2O	bdl	bdl	bdl	bdl	bdl	bdl	bdl	bdl	bdl	bdl	bdl	bdl
K_2O	bdl	bdl	bdl	bdl	bdl	bdl	bdl	bdl	bdl	bdl	bdl	bdl
Total	85.46	85.03	88.70	83.74	82.57	88.24	84.16	85.46	88.02	84.12	87.92	87.69
LOI[a]	14.54	14.97	11.30	16.26	17.44	11.76	15.84	14.54	11.98	15.89	12.08	12.31
Ni (ppm)	2223	2293	2142	2186	2610	2205	2244	2209	2277	2154	2064	2205
V	40	41	50	39	37	35	36	34	32	41	58	50
Cr	2394	3467	3633	2824	2605	1520	2769	2327	2484	2437	3217	3572
Li	0.45	0.36	0.7	0.31	0.28	0.66	0.26	0.23	0.40	0.29	1.2	0.7
Co	99	82	91	97	105	98	102	97	97	101	100	86
Rb	0.026	0.023	0.016	0.053	0.024	0.036	0.036	0.014	0.027	0.043	0.016	0.021
Sr	0.36	0.7	1.1	0.19	1	0.16	0.40	0.18	1.9	0.18	1.0	0.48
Zr	0.027	0.10	0.021	0.09	0.022	0.053	0.022	0.060	0.10	0.0683	1.1	1.3
Nb	0.0060	0.0034	0.0041	0.011	0.015	bdl	0.017	0.0043	0.0065	0.009	0.016	0.026
Cs	0.0039	0.0016	0.0021	0.0041	0.0027	0.0021	0.0036	0.0013	0.0024	0.0016	0.0040	0.0017
La	bdl	bdl	bdl	bdl	bdl	bdl	bdl	bdl	bdl	bdl	bdl	bdl
Ce	0.0037	0.0036	0.0025	0.0020	0.0019	0.0029	0.0049	0.0033	0.0029	0.0017	0.17	0.14
Nd	0.0044	0.0031	0.0053	0.0021	0.009	0.0032	0.0041	0.0029	0.0022	0.0024	0.17	0.16
Sm	bdl	bdl	bdl	bdl	bdl	bdl	bdl	bdl	bdl	bdl	0.065	0.061
Eu	bdl	bdl	bdl	bdl	bdl	bdl	0.0008	bdl	bdl	0.0007	0.036	0.031
Gd	bdl	bdl	bdl	bdl	0.0028	bdl	bdl	0.0036	0.0021	bdl	0.13	0.11
Tb	0.0004	0.0002	bdl	0.0006	0.0004	0.0009	0.0007	0.0006	0.0004	bdl	0.024	0.020
Dy	0.0048	0.0041	0.007	0.0057	0.0035	0.011	0.0051	0.0045	0.0037	0.0036	0.18	0.16
Ho	0.0019	0.0016	0.0026	0.0020	0.0013	0.0039	0.0017	0.0017	0.0015	0.0016	0.042	0.034
Er	0.009	0.007	0.012	0.010	0.0063	0.014	0.009	0.010	0.008	0.009	0.12	0.10
Tm	0.0022	0.0019	0.0031	0.0023	0.0018	0.0033	0.0022	0.0023	0.0022	0.0022	0.019	0.016
Yb	0.022	0.017	0.029	0.020	0.016	0.026	0.021	0.022	0.020	0.021	0.13	0.11
Lu	0.0050	0.0039	0.007	0.0046	0.0044	0.0054	0.0050	0.0054	0.0050	0.0058	0.022	0.018
Hf	bdl	0.0041	bdl	0.0022	0.0022	0.0026	bdl	0.0026	0.0029	0.0023	0.038	0.043
Ta	bdl	bdl	bdl	0.0016	0.0018	bdl	0.0020	0.0005	0.0008	0.0003	0.0013	0.0018
Th	0.0034	0.0006	0.0039	bdl	0.0009	0.0015	0.0014	0.0006	0.0007	0.0026	0.0014	0.0017
U	bdl	0.0004	bdl	0.0013	bdl	bdl	bdl	bdl	bdl	bdl	0.0014	0.0009

bdl Below detection limit, *CG* Cayo Guam section, *YM* Yamaniguey section, *LB* Loma de la Bandera section, *LEM* Loma Estrella Mayarí section, *LAS* Loma Arroyo Seco section

[a]Reported loss on ignition is not the measured LOI but an estimate assuming that primary major oxide totals are equal to 100

and Ta concentrations were determined by using Zr and Hf, respectively, as internal standards. This technique is an implementation to ICP-MS analysis of the method described by Jochum et al. (1990). Detection limits obtained by long-term (several years) analyses of chemical blanks at ISTEEM can be found in Ionov et al. (1992) and Garrido et al. (2000).

Because of the extremely low concentrations of some incompatible trace elements in most MBOB peridotites we took special care in their analyses. Only extra clean Teflon® beakers were used to minimize contamination during sampling dissolution and lower chemical blank corrections. The assessment of the analysis precision of a given element was made using 3-run measurements in the same solution and estimating the standard deviation (σ_s) from the standard deviations of the sample (σ_s), instrumental (σ_i) and procedural blank (σ_p) measurements as: $\sigma_s = \sqrt{\sigma_i^2 + \sigma_p^2 + \sigma_s^2}$ (see Godard et al. 2000). The analysis was discarded when $\sigma_s > 80\%$ of the mean. In addition, duplicate analyses were performed for several highly depleted samples. The composition of the reference samples (PCC-1, UB-(n), BHVO-1 and BIR) (Table 3), analysed as an unknown during the same analytical runs as MBOB samples, shows good agreement with working values for these reference samples (Govindaraju 1994). For the analysed elements, reproducibility of these references samples is generally better than 10% for UB-(n), BHVO-1 and BIR, and within 5–35% for PCC-1.

In situ trace element analyses of cpx were carried out by LA-ICP-MS in approximately 150 μm thick

Table 1 (Contd.)

				Mayarí-Cristal massif									
				North				South					
				Harzburgite				Harzburgite			Dunite		
CG 4	CG 18	YM 12	YM 13	LB 2	LB 3	LB 5	LB 6	LEM 1	LEM 2	LEM 3	LAS 2	LAS 1	LEM 4
37.01	36.79	34.57	35.86	39.67	39.07	44.63	41.16	39.93	39.39	39.24	39.71	39.33	39.62
0.08	0.08	0.02	0.01	0.008	0.006	0.008	0.006	0.004	0.003	0.003	0.004	0.004	0.005
1.94	2.57	0.89	0.54	0.52	0.58	0.43	0.44	0.27	0.19	0.17	0.12	0.05	bdl
8.91	9.34	8.76	8.25	7.94	8.08	9.00	8.52	7.99	7.93	8.57	8.03	7.40	9.24
0.12	0.13	0.12	0.08	0.08	0.08	0.11	0.09	0.10	0.11	0.11	0.11	0.09	0.11
39.41	39.10	39.64	38.42	37.63	35.46	40.82	35.95	35.40	35.23	33.71	36.13	36.55	33.84
1.13	1.86	0.15	0.02	0.03	n.d.	0.04	0.07	0.02	0.17	0.04	0.06	0.01	0.02
bdl	bdl	bdl	bdl	bdl	bdl	bdl	bdl	bdl	bdl	bdl	bdl	bdl	bdl
bdl	bdl	bdl	bdl	bdl	bdl	bdl	bdl	bdl	bdl	bdl	bdl	bdl	bdl
88.60	89.86	84.15	83.19	85.87	83.28	95.04	86.24	83.71	83.02	81.85	84.16	83.44	82.84
11.40	10.14	15.85	16.82	14.13	16.72	4.96	13.76	16.29	16.98	18.15	15.84	16.56	17.16
1473	1743	2505	2428	2163	2109	2484	2418	2238	2212	2533	2234	2724	2659
42	49	40	25	48	38	30	34	30	26	26	38	15	35
1547	2251	3462	4457	2618	2437	2730	2052	2623	2449	3069	2605	3173	5003
1.4	1.9	0.26	0.038	0.26	0.31	0.24	0.39	0.27	0.24	0.32	0.26	0.13	0.19
116	108	109	110	92	95	100	103	96	97	108	97	112	119
0.014	bdl	bdl	0.10	0.031	0.048	0.022	0.040	0.019	0.022	0.029	0.030	0.019	0.030
0.7	2.6	0.24	0.16	0.48	0.7	0.33	1.0	0.41	0.55	0.9	0.7	0.7	0.8
2.1	3.8	0.31	0.17	0.18	0.16	0.036	0.32	0.19	0.12	0.056	0.049	0.10	0.040
0.018	0.036	0.0044	0.013	0.013	0.011	0.009	0.010	0.011	0.011	0.012	0.011	0.015	0.026
0.0023	bdl	bdl	bdl	0.0019	0.0050	0.0031	0.0037	0.0052	0.0062	0.009	0.0058	0.0052	0.009
bdl	bdl	bdl	bdl	bdl	0.0007	bdl	bdl	bdl	bdl	bdl	bdl	bdl	bdl
0.31	0.47	0.039	0.044	0.0036	0.0058	0.0021	0.0024	0.0017	0.0016	0.0021	0.0038	0.0016	0.0033
0.32	0.44	0.040	0.024	0.0033	0.009	0.0037	0.022	0.010	0.0031	0.0030	0.0043	0.0023	0.0031
0.11	0.14	0.017	bdl	bdl	0.0049	bdl	0.007	0.0036	bdl	bdl	bdl	0.0021	bdl
0.057	0.059	0.009	0.011	0.0011	0.0017	bdl	0.0026	0.0013	bdl	bdl	bdl	0.0006	0.0005
0.19	0.20	0.029	0.008	0.0053	0.007	bdl	0.013	0.0059	bdl	bdl	bdl	0.0027	bdl
0.033	0.037	0.0058	0.0012	0.0012	0.0015	0.0006	0.0015	0.0005	0.0003	0.0006	0.0005	0.0005	0.0005
0.26	0.26	0.045	0.008	0.013	0.014	0.0040	0.012	0.0029	0.0020	0.0044	0.0027	0.0036	0.0033
0.057	0.059	0.011	0.0024	0.0043	0.0045	0.0018	0.0043	0.0012	0.0010	0.0014	0.0007	0.0012	0.0011
0.17	0.17	0.037	0.008	0.017	0.018	0.011	0.017	0.0056	0.0052	0.0057	0.0039	0.0054	0.0038
0.026	0.026	0.0066	0.0013	0.0031	0.0038	0.0021	0.0035	0.0013	0.0012	0.0013	0.0009	0.0011	0.0010
0.18	0.18	0.048	0.011	0.030	0.034	0.023	0.030	0.014	0.013	0.012	0.010	0.010	0.010
0.032	0.031	0.009	0.0029	0.0062	0.007	0.0051	0.007	0.0035	0.0032	0.0031	0.0027	0.0024	0.0022
0.08	0.14	0.012	0.0054	0.0062	0.008	0.0052	0.008	0.0045	0.0038	0.0047	0.0063	0.008	0.007
0.0019	0.0033	bdl	0.0019	bdl	0.0013	0.0013	0.0015	0.0014	0.0015	0.0011	0.0013	0.0017	0.0017
0.0020	0.0027	0.0007	0.0017	0.0009	0.0008	0.0006	0.0005	0.0008	0.0006	0.0006	0.0006	0.0008	0.0006
0.0009	0.0008	bdl	0.0024	0.0007	0.0014	0.0009	0.0006	0.0005	0.0005	0.0007	0.0006	0.0004	0.0007

sections for two Moa-Baracoa crustal gabbros. Analyses have been performed at ISTEEM using a VG-PQ2 Turbo + ICP-MS, coupled with a Geolas (Microlas) automated platform housing a 193 nm Compex 102 laser from LambdaPhysik. Signals were acquired in Time Resolved Acquisition (TRA), devoting 2 min for the blank and 1 min for measurement of the analytes. The laser was fired using an energy density of 15 J/cm^2 at a frequency of 5 Hz and using a spot size of 77 μm. The drilling rate was around 0.15 μm/pulse, which, under the analytical conditions used in this study, resulted in crater depths of about 45 μm. ^{30}Si was used as an internal standard and analyte concentrations were calibrated against the NIST 610 rhyolitic glass, which was measured each five unknowns. LA-ICP-MS data are given in Table 4.

Mineral chemistry

Peridotites

In Moa-Baracoa harzburgite, the Mg# [$100 \times$ Mg/(Mg + Fe^{2+})] of ol and the Cr# [Cr/(Cr + Al)] of spinel vary between 90.3–90.9 (Fig. 3a) and 0.45–0.55 (Fig. 3b), respectively; opx has an average Mg# = 91.1 and Al$_2$O$_3$ = 2.4 wt%. Mg# of ol in Moa-Baracoa dunite is slightly higher (90.7–91.5) than that of harzburgite, whereas Cr# of spinel is similar (0.51–0.52). Impregnated dunite has ol with lower Mg# (88.7–90.0) and spinel with slightly higher Cr# (up to 0.59) than the other peridotites from Moa-Baracoa; spinel also shows significant enrichment in FeO and mainly TiO$_2$ (1.3–2.0 wt%) (Fig. 3d, e). Secondary cpx in impregnated

Table 2 Whole rock major and trace element data of gabbroic rocks from the Mayarí-Baracoa Ophiolitic Belt

Location   Moa-Baracoa massif

	Crustal gabbros (Layered gabbros)															Sills in the MTZ	
Rocktype	Olivine gabbro											Ol-opx-gabbro			Gabbro	Olivine gabbro	
Sample	QN 21	QN 18	QN 16	QN 12	QN 11b	QN 10a	QN 10b	QN 8	QN 5	QN 2	QN 1	QN 9	QN 7	QN 4	QN 14	YM 3	YM 4
SiO_2 (wt%)	46.40	45.99	47.02	48.16	46.45	47.26	45.82	47.71	49.56	48.32	47.49	45.53	42.81	50.00	49.85	39.00	40.28
TiO_2	0.20	0.19	0.26	0.20	0.16	0.21	0.11	0.19	0.24	0.24	0.23	0.09	0.11	0.29	0.31	0.12	0.26
Al_2O_3	17.96	20.41	16.86	21.31	25.66	23.13	20.58	22.89	17.59	17.31	17.62	22.20	15.02	16.85	18.89	4.06	6.45
Fe_2O_3	7.87	5.18	6.44	5.05	3.88	5.31	7.85	4.17	6.20	6.26	5.94	6.73	10.22	6.10	4.39	19.16	16.51
MnO	0.11	0.08	0.10	0.08	0.05	0.07	0.10	0.07	0.11	0.11	0.10	0.08	0.14	0.11	0.09	0.26	0.23
MgO	11.39	8.43	11.81	7.95	5.15	7.48	10.49	6.44	11.23	11.47	10.84	8.72	16.20	11.05	7.36	26.55	22.43
CaO	12.43	13.19	13.73	13.39	12.08	11.90	10.24	13.16	15.17	14.79	14.38	10.47	8.62	15.71	14.61	3.43	6.01
Na_2O	1.36	1.85	1.38	2.04	2.40	2.22	1.90	2.15	1.43	1.30	1.29	2.08	1.25	1.37	2.17	0.18	0.50
K_2O	bdl	bdl	bdl	0.01	0.01	0.01	bdl	0.01	bdl	bdl	bdl	0.01	bdl	bdl	0.01	bdl	bdl
Total	97.72	95.33	97.60	98.20	95.84	97.59	97.09	96.79	101.53	99.80	97.90	95.91	94.36	101.48	97.68	92.77	92.67
LOI[a]	2.28	4.67	2.40	1.80	4.16	2.41	2.92	3.21		0.20	2.10	4.09	5.64		2.32	7.23	7.33
Ni (ppm)	278	169	220	217	159	254	408	154	234	279	258	322	472	243	124	907	761
V	88	95	116	77	22	46	26	88	138	140	121	41	42	157	148	63	97
Cr	393	346	655	639	32	155	88	487	797	869	712	56	268	855	1083	220	450
Li	1.5	2.2	1.7	1.8	2.0	2.2	2.2	1.9	1.1	1.7	1.7	2.4	2.2	1.4	2.1	1.8	2.8
Co	53	33	43	29	24	32	52	24	41	42	41	42	79	40	19	126	108
Rb	0.10	0.16	0.09	0.08	0.05	0.06	0.08	0.05	0.03	0.04	0.04	0.09	0.06	0.05	0.14	0.057	0.09
Sr	80	99	113	141	171	157	135	139	87	76	80	149	81	78	132	17	47
Zr	5.9	5.1	6	5	7	7	5	5	4	4	4	4	3	5	6	2.0	9
Nb	0.08	0.10	0.09	0.09	0.23	0.26	0.06	0.09	0.04	0.05	0.04	0.07	0.05	0.05	0.05	0.019	0.22
Cs	0.0028	0.0033	0.0031	0.0039	0.0017	0.0017	0.0019	0.0013	0.0018	0.0024	0.0037	0.0023	0.0017	0.0032	0.0027	0.0037	0.0059
La	0.26	0.25	0.29	0.29	0.34	0.38	0.24	0.29	0.23	0.24	0.23	0.25	0.20	0.26	0.27	0.09	0.40
Ce	0.9	0.8	1.0	0.9	1.1	1.2	0.7	0.9	0.8	0.8	0.8	0.7	0.6	0.9	1.0	0.30	1.2
Nd	1.0	0.9	1.2	1.0	0.9	1.0	0.6	0.9	1.0	1.1	1.1	0.6	0.6	1.3	1.3	0.40	1.3
Sm	0.40	0.37	0.53	0.40	0.26	0.34	0.19	0.35	0.48	0.49	0.49	0.17	0.20	0.59	0.61	0.19	0.54
Eu	0.28	0.30	0.35	0.34	0.33	0.34	0.26	0.34	0.35	0.35	0.36	0.28	0.23	0.38	0.40	0.13	0.28
Gd	0.63	0.58	0.88	0.65	0.36	0.45	0.27	0.55	0.83	0.85	0.85	0.23	0.32	1.02	1.07	0.35	0.9
Tb	0.12	0.11	0.16	0.12	0.06	0.08	0.05	0.10	0.16	0.16	0.16	0.04	0.06	0.19	0.20	0.07	0.16
Dy	0.9	0.8	1.2	0.9	0.4	0.5	0.3	0.7	1.2	1.2	1.2	0.3	0.4	1.4	1.5	0.52	1.2
Ho	0.18	0.17	0.25	0.18	0.09	0.11	0.07	0.16	0.25	0.25	0.25	0.05	0.09	0.30	0.32	0.12	0.26
Er	0.52	0.47	0.70	0.50	0.24	0.31	0.18	0.43	0.70	0.70	0.69	0.15	0.26	0.83	0.88	0.36	0.8
Tm	0.08	0.07	0.10	0.07	0.03	0.04	0.03	0.06	0.10	0.10	0.10	0.02	0.04	0.12	0.12	0.054	0.11
Yb	0.49	0.43	0.63	0.45	0.22	0.29	0.19	0.39	0.62	0.63	0.62	0.14	0.25	0.75	0.78	0.38	0.7
Lu	0.08	0.07	0.10	0.07	0.03	0.05	0.03	0.06	0.10	0.10	0.10	0.02	0.04	0.12	0.12	0.07	0.13
Hf	0.20	0.17	0.24	0.18	0.20	0.19	0.14	0.15	0.18	0.20	0.19	0.11	0.09	0.24	0.23	0.09	0.32
Ta	0.007	0.007	0.007	0.006	0.016	0.017	0.006	0.007	0.011	0.012	0.015	0.006	0.011	0.013	0.003	0.0020	0.016
Th	0.005	0.005	0.006	0.005	0.009	0.007	0.006	0.006	0.002	0.002	0.002	0.005	0.004	0.003	0.003	0.0022	0.014
U	0.0022	0.0025	0.0022	0.0021	0.0045	0.0033	0.0019	0.0021	0.0006	0.0009	0.0007	0.0023	0.0018	0.0014	0.0012	0.0009	0.0054

bdl Below detection limit, *NA* not analysed, *QN* Quemado del Negro section, *YM* Yamaniguey section, *AM* Amores section, *CG* Cayo Guam section, *MER& J* Mercedita section, *LB* Loma de la Bandera section

[a]Loss on ignition (LOI) was not measured except for Moa-Baracoa dykes; LOI values reported for the other samples are estimations assuming that primary major oxide totals were equal to 100

dunite exhibits Mg# ranging from 88.6 to 91.6, and average Al_2O_3 = 3.5 wt% and TiO_2 = 1.3 wt%.

Owing to pervasive serpentinization, we were unable to analyse ol and opx in Mayarí-Cristal harzburgites. Spinel exhibits generally higher Cr# (from 0.53 to 0.67) (Fig. 3b) than that from Moa-Baracoa harzburgite in particular in the southern tectonites, where it is also enriched in FeO (Fig. 3d). The Mg# of ol in Mayarí-Cristal dunites ranges from 91.9 to 92.4 (Fig. 3a); spinel displays Cr# that varies between 0.59–0.75 (Fig. 3b) and TiO_2 (average value = 0.12 wt%) notably higher than in peridotites from the other regions of the MBOB (Fig. 3e).

The range of ol Mg# in MBOB peridotites overlaps that of both ocean ridge and supra-subduction zone peridotites (Fig. 3a) and more generally fits in the data commonly reported for mantle rocks. This is also true for the Cr# of spinel except for the high values displayed by peridotites from southern Mayarí-Cristal massif that are characteristic only of spinel from supra-subduction settings (Fig. 3b) (Pearce et al. 2000).

Gabbros

Olivine, opx and cpx in gabbroic rocks from Moa-Baracoa exhibit Mg# values (74.0–82.6 in ol, 77.4–82.7

Table 2 (Contd.)

																Mayarí-Cristal northern domain	
										Intrusive Dykes in the MTZ						Dykes	
			Ol-opx-gabbro					Trocto-lite	Werh-lite	Olivine-gabbro				Trocto-lite	Werh-lite	Gabbro	Px-Hbl-gabbro
YM 5	YM 7	YM10b	YM10c	YM10d	YM10e	AM 14	CG 17	MER 1	YM 10a	CG 4b	CG 5b	CG 7b	J 3b	CG 9b	J 2b	LB 1	LB 4
37.23	39.53	39.35	46.74	41.88	38.77	48.83	41.06	37.27	38.39	39.75	45.50	42.20	46.46	39.33	38.13	45.18	41.76
0.03	0.04	0.10	0.45	0.16	0.09	0.26	0.21	0.01	0.11	0.09	0.17	0.16	0.16	0.07	0.06	0.45	1.14
11.49	20.42	12.50	7.63	17.99	5.56	16.91	6.30	5.36	3.05	18.33	10.52	13.29	18.66	10.74	6.53	15.23	15.85
6.56	4.50	11.02	11.15	7.21	15.84	6.83	12.73	9.71	17.03	5.76	5.47	4.76	4.66	8.67	7.87	8.56	7.19
0.10	0.06	0.16	0.22	0.10	0.21	0.12	0.19	0.13	0.22	0.09	0.12	0.10	0.08	0.13	0.12	0.15	0.12
26.10	14.65	20.77	17.43	13.99	27.71	9.89	27.59	36.71	30.78	17.63	17.78	20.66	13.01	30.90	36.25	10.77	10.64
7.28	11.24	7.51	12.09	10.91	4.30	13.20	5.19	2.21	2.84	10.96	15.34	12.35	12.58	5.48	2.53	13.78	16.82
bdl	0.49	0.57	0.72	1.23	0.16	1.98	0.45	0.03	0.06	bdl	bdl	bdl	1.51	bdl	0.07	1.26	0.31
bdl	0.03	bdl	0.01	bdl	0.02	bdl	bdl	bdl	bdl	bdl	bdl	bdl	bdl	bdl	0.02	bdl	bdl
88.79	90.96	91.99	96.42	93.48	92.64	98.03	93.72	91.44	92.47	92.61	94.90	93.52	97.12	95.32	91.56	95.40	93.85
11.21	9.04	8.01	3.58	6.52	7.36	1.97	6.29	8.56	7.53	6.94	4.24	6.18	2.67	5.95	8.69	4.60	6.15
1034	544	664	435	373	933	184	1400	1857	1005	NA	NA	NA	NA	NA	n.a.	120	195
33	35	44	231	55	46	130	108	30	66	NA	NA	NA	NA	NA	n.a.	278	265
1488	771	229	1535	166	398	409	2275	3414	505	NA	NA	NA	NA	NA	n.a.	247	285
1.0	2.4	3.7	1.6	1.4	2.0	1.7	2.1	2.4	1.0	17	12	15	3	10	2	15	21
73	51	84	68	53	114	49	88	111	125	54	40	43	41	90	100	45	38
0.07	0.19	0.10	0.09	0.15	0.051	0.13	0.09	0.18	0.033	0.48	0.14	0.21	0.44	0.16	0.25	0.28	0.28
3.9	58	45	37	77	21	125	38	18	5.9	32	20	34	163	14	34	202	62
0.7	3.0	2.0	13	3.5	0.9	4.7	3.5	0.10	2.3	1.6	3.7	3.5	3.2	2.0	2.3	6.2	23
0.016	0.07	0.020	0.08	0.045	0.019	0.051	0.012	0.013	0.027	0.08	0.060	0.050	0.040	0.07	0.25	0.07	0.8
0.003	0.0057	0.008	0.0060	0.009	0.0019	bdl	0.007	0.008	bdl	0.07	0.10	0.020	0.040	0.030	0.23	0.27	0.012
0.029	0.063	0.15	0.38	0.27	0.063	0.26	0.16	bdl	0.07	0.20	0.15	0.24	0.18	0.14	0.10	0.35	1.6
0.057	0.19	0.48	1.6	0.8	0.21	0.9	0.56	0.041	0.28	0.30	0.48	0.9	0.46	0.34	0.28	1.4	6.2
0.066	0.21	0.50	2.3	0.8	0.30	1.3	0.8	0.032	0.42	0.35	0.63	0.7	0.66	0.24	0.27	1.8	8
0.026	0.09	0.18	1.1	0.31	0.14	0.57	0.34	0.010	0.20	0.18	0.36	0.37	0.32	0.07	0.14	0.8	3.2
0.026	0.065	0.13	0.47	0.30	0.12	0.40	0.21	0.025	0.11	0.13	0.17	0.23	0.28	0.051	0.07	0.43	1.1
0.053	0.13	0.29	1.9	0.47	0.25	1.0	0.59	0.015	0.37	0.31	0.65	0.7	0.55	0.14	0.19	1.2	4.8
0.012	0.023	0.053	0.36	0.08	0.048	0.18	0.11	0.003	0.07	0.057	0.14	0.13	0.10	0.029	0.033	0.24	0.9
0.11	0.17	0.39	2.7	0.61	0.36	1.4	0.9	0.020	0.52	0.39	1.0	0.9	0.7	0.23	0.20	1.8	6.3
0.026	0.038	0.08	0.57	0.13	0.08	0.30	0.19	0.0050	0.12	0.09	0.24	0.21	0.16	0.062	0.040	0.41	1.4
0.09	0.11	0.25	1.7	0.37	0.24	0.79	0.56	0.021	0.35	0.26	0.7	0.57	0.44	0.21	0.10	1.2	3.7
0.014	0.016	0.038	0.24	0.055	0.037	0.12	0.08	0.0041	0.053	0.040	0.11	0.09	0.065	0.034	0.016	0.17	0.54
0.11	0.10	0.25	1.53	0.37	0.26	0.7	0.56	0.037	0.35	0.26	0.7	0.54	0.37	0.24	0.10	1.1	3.3
0.019	0.017	0.045	0.24	0.060	0.047	0.12	0.09	0.008	0.063	0.038	0.10	0.08	0.054	0.040	0.015	0.18	0.53
0.020	0.09	0.10	0.52	0.13	0.051	0.24	0.16	0.0039	0.11	0.08	0.17	0.17	0.19	0.060	0.12	0.32	1.3
0.0014	0.0058	0.0015	0.0063	0.0046	0.0005	0.016	0.0012	0.0015	0.0019	0.020	0.010	0.010	0.010	0.020	0.040	0.0157	0.065
0.0008	0.0039	0.0010	0.007	0.0029	bdl	0.0037	0.0006	0.0005	0.0016	0.016	0.012	0.009	0.0050	0.007	0.07	0.0046	0.037
bdl	0.0016	0.00001	0.0028	0.0011	bdl	0.0021	bdl	bdl	0.0008	0.0030	0.002	0.0020	0.0040	0.0030	0.008	0.0035	0.020

in opx and 78.8–91.7 in cpx) comparable to similar ophiolitic (e.g. Korenaga and Kelemen 1997) and oceanic gabbroic rocks. Anorthite (An) content in plagioclase varies between 63–71, 68–70 and 66–76 wt% in sills, dykes and layered gabbros, respectively.

Clinopyroxene in mafic dykes from the Mayarí-Cristal northern domain exhibits a Mg# average value = 81.2. Plagioclase is remarkably richer in Ca (An$_{80–87}$) compared to Moa-Baracoa gabbroic rocks (Fig. 3c).

The An content of plagioclase in Moa-Baracoa gabbros is characteristic of gabbros crystallized at ocean spreading centres (An = 48–97 wt%, according to Beard 1986), whereas that of plagioclase from Mayarí-Cristal gabbro dyke is compatible with both ocean ridge and arc setting (An = 78–100 wt%, according to Beard 1986) (Fig. 3c).

Whole rock geochemistry

Peridotites

The analysed major oxide totals of MBOB peridotites range from 82 to 95 wt% indicating significant addition of volatile components during alteration (Table 1). Owing to the lack of mineral analyses for all mineral phases, we were unable to reconstruct the major element whole rock compositions combining modes and mineral chemistry as customarily done for abyssal peridotites (e.g. Dick 1989; Niu et al. 1997; Baker and Beckett 1998; Asimow 1999).

Mayarí-Baracoa Ophiolitic Belt peridotites show low Al$_2$O$_3$ contents (< 1.2 anhydrous wt%) and are highly

Table 3 Trace element contents of international reference samples analysed in this study

Standard runs	PCC-1 ($n = 3$)	RSD (%)	UB-(n) ($n = 11$)	RSD (%)	BHVO-1 ($n = 8$)	RSD (%)	BIR ($n = 2$)	RSD (%)
Rb (ppm)	0.07	10	3.4	5	9	4	0.19	3
Sr	0.40	5	8	4	352	7	73	9
Zr	0.14	15	3.6	7	165	5	14	6
Nb	0.027	5	0.057	14	18	3	0.61	1
Cs	0.008	5	11	4	0.10	6	0.0054	8
La	0.033	6	0.33	4	15	2	0.66	1
Ce	0.051	5	0.83	5	39	2	1.9	1
Nd	0.028	9	0.63	6	26	4	2.4	2
Sm	0.015	23	0.218	5	6.1	3	1.1	2
Eu	0.003	26	0.081	6	2.1	5	0.54	1
Gd	0.011	16	0.33	5	6.4	4	1.9	2
Tb	0.0018	19	0.062	5	1.0	5	0.37	2
Dy	0.021	19	0.46	6	5.8	5	2.8	3
Ho	0.0048	12	0.101	6	1.1	6	0.61	2
Er	0.0159	12	0.298	4	2.6	5	1.8	2
Tm	0.0032	15	0.045	6	0.34	5	0.26	2
Yb	0.026	8	0.299	5	2.0	5	1.7	1
Lu	0.0061	9	0.050	6	0.30	6	0.27	2
Hf	0.008	33	0.14	6	4.7	7	0.64	2
Ta	0.0031	34	0.019	16	1.2	8	0.040	1
Th	0.013	10	0.07	15	1.3	7	0.035	1
U	0.0084	19	0.058	13	0.44	9	0.012	10

Values are average contents of "*n*" analyses of a given reference sample. RSD% are the variation coefficient in percentage. At least one reference sample was measured as an unknown in each analytical run
PCC-1 Dunite, *UBN* Serpentinite, *BHVO-1* Basalt, *BIR* Basalt

Table 4 Average EMPA and LA-ICP-MS analyses of cpx in Moa-Baracoa Crustal Gabbro

	QN 2 ($n = 12$)	RSD (%)	QN 4 ($n = 15$)	RSD (%)
SiO$_2$	52.15	1	51.48	0.4
TiO$_2$	0.69	11	0.63	6
Al$_2$O$_3$	2.46	5	2.33	4
Fe$_2$O$_3$	2.39	15	1.03	7
Cr$_2$O$_3$	0.36	11	0.31	8
FeO	4.49	32	5.23	7
MgO	17.05	9	15.81	4
CaO	20.47	12	22.32	4
Na$_2$O	0.35	16	0.34	12
Total	100.41	1	99.48	0.3
Sr (ppm)	4.6	7	4.4	21
Y	16	5	17	10
Zr	10	9	12	15
Nb	0.07	35	0.11	33
La	0.21	6	0.26	19
Ce	1.4	8	1.6	15
Nd	2.5	10	2.7	14
Sm	1.3	12	1.3	15
Eu	0.48	9	0.49	15
Gd	2.2	8	2.2	16
Tb	0.41	7	0.41	14
Dy	3.0	7	3.0	14
Ho	0.64	6	0.65	13
Er	1.8	7	1.9	13
Tm	0.26	7	0.28	12
Yb	1.8	7	1.8	9
Lu	0.25	6	0.27	12
Hf	0.43	18	0.48	23

Values are average contents of "*n*" analyses
RSD (%) Relative standard deviation (percentage)

refractory mantle rocks (Fig. 4a–c); in particular, the southern Mayarí-Cristal samples exhibit the lowest Al$_2$O$_3$ abundances (Fig. 4d–f). SiO$_2$ and (to a lesser extent) FeOt contents are higher than values usually reported for oceanic peridotites (Fig. 4a, b). As generally noted for mantle tectonites (e.g. Bodinier and Godard 2003) the Al$_2$O$_3$ content of MBOB peridotites is correlated with TiO$_2$ (Fig. 4f) and Yb (Fig. 5). Impregnated dunites are located out of these trends most likely owing to peridotite refertilization.

The chondrite-normalized REE patterns of MBOB ultramafics are displayed in Fig. 6. The rock/chondrite REE concentrations for the peridotites are very low, ranging between 0.002–0.05 and 0.005–0.3 for LREE and HREE, respectively. The patterns have strikingly homogenous HREE contents and are characterized by relatively flat LREE and steep HREE fractionated segments. These REE patterns are similar to those of abyssal peridotites from Izu-Bonin-Mariana forearc (Parkinson and Pearce 1998) (Fig. 6a, b) and to those of the most depleted harzburgites from Oman ophiolite (Godard et al. 2000). The Mayarí-Cristal southern domain is depleted in MREE and HREE compared to the northern one, whereas Moa-Baracoa massif has generally intermediate concentrations. Comparing these results with those published by Proenza et al. (1999b) on Mayarí-Baracoa peridotites associated with chromitite ore deposits, our samples display significantly lower LREE and MREE and nearly identical HREE contents. Impregnated dunites from Moa-Baracoa

Fig. 3 a Mg# ranges of olivine from MBOB peridotites; **b** Cr# ranges of chromian spinel from MBOB peridotites; **c** Anorthite contents (wt%) of plagioclase from MBOB gabbros. *Horizontal bar within columns* marks the average value. *1* Moa-Baracoa harzburgite, *2* Moa-Baracoa dunite, *3* Moa-Baracoa impregnated dunite, *4* Mayarí-Cristal northern harzburgite, *5* Mayarí-Cristal southern harzburgite, *6* Mayarí-Cristal southern dunite, *7* Moa-Baracoa gabbro, *8* Mayarí-Cristal gabbro dyke, *9* arc (supra-subduction zone) peridotite or gabbro (in **c**), *10* ocean ridge peridotite or gabbro (in **c**). Data of columns 9 and 10 are from Pearce et al. (2000) and Beard (1986) (in **c**), and references therein. **d** Cr# vs. Mg# of chromian spinel from MBOB mantle peridotites. Fields for MORB, back-arc basalts and Lau basin island arc tholeiites (IAT) are from Metzger et al. (2002), and references therein. **e** Average Cr# vs. average TiO_2 content of chromian spinel from MBOB mantle peridotites; *bars* represent standard deviations from average values. *Symbols* as in Fig. 2a
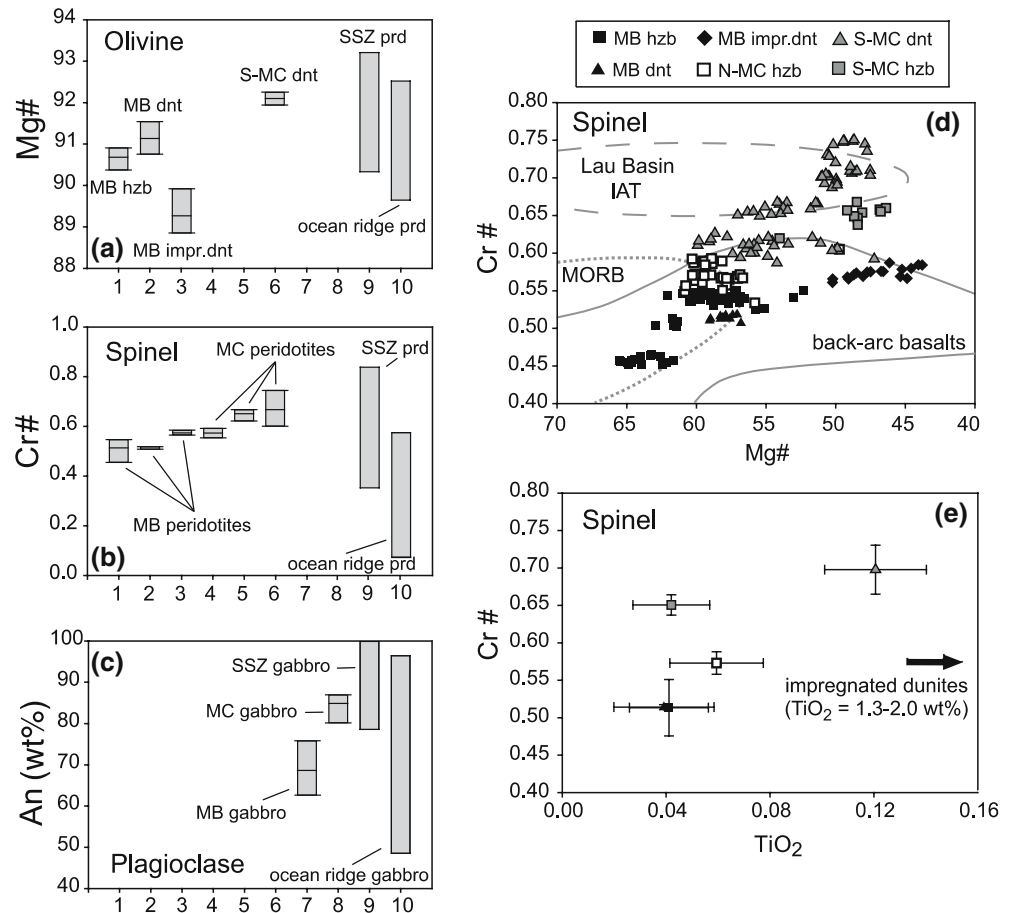
massif display higher REE contents than the other ultramafics and generally flat patterns occasionally associated with a positive anomaly in Eu (Fig. 6c). These patterns are consistent with secondary precipitation of cpx and plagioclase in variable amounts.

The distribution of lithophile trace elements (REE, Cs, Rb, Th, U, Nb, Ta, Sr, Zr, and Hf) normalized to primitive mantle for MBOB ultramafics is shown in Fig. 7. MBOB peridotites are highly depleted in terms of lithophile trace elements. Nevertheless, they exhibit variable relative enrichment in the most incompatible trace elements (Cs to Ta) and low LREE/HREE fractionation. Sr shows a positive spike particularly prominent for Moa-Baracoa peridotites. Zr and Hf are commonly enriched relative to LREE. Mayarí-Cristal tectonites are more depleted in Th and richer in Zr and Hf than Moa-Baracoa ones. Impregnated dunites exhibit higher average content of lithophile elements (except for Cs, Rb, Th and Sr) and flatter normalized patterns than the other ultramafics. Cs, Rb, U and Sr are commonly considered highly mobile during alteration of mantle rocks (Niu 2004) and their budgets are generally believed to be affected by late circulation of aqueous solutions; for this reason they will not be treated in the following discussion. Nevertheless it should be noted that all MBOB peridotites lack the

high U/Th ratios indicative of low-temperature oxidative alteration (Pearce et al. 2000).

Gabbros

The degree of alteration of MBOB sills, dykes and layered gabbros is rather variable as indicated by LOI values, and generally higher in sills and dykes than in layered gabbros. Among the samples from Moa-Baracoa, sills and dykes are richer in MgO and poorer in SiO_2, Al_2O_3 and CaO than layered gabbros (Fig. 8). One dyke from the Mayarí-Cristal massif has a whole rock composition similar to those of Moa-Baracoa samples, whereas the other shows higher CaO owing to the abundance of primary calcic-amphibole; this dyke is also enriched in TiO_2 (1.2 anhydrous wt%) because of the abundance of Ti oxide and amphibole.

The chondrite-normalized REE patterns of Moa-Baracoa layered gabbros display LREE-depleted to relatively flat REE patterns with homogenous LREE contents, sharp positive Eu anomalies, and variable HREE contents (Fig. 9a). These patterns suggest that gabbros are cumulates from variably fractionated melts (Kelemen et al. 1997). MBOB sills and dykes are characterized by depleted or flat LREE concentrations,

Fig. 4 a–c Whole rock abundances of SiO₂, FeOt, and TiO₂ versus Al₂O₃ in Mayarí-Baracoa ultramafics and published data (*grey circles*) for peridotites from different tectonic settings (Bodinier and Godard 2003 and references therein). **d–f** Enlarged area of previous plots in order to display MBOB data in more detail. All data on anhydrous basis in wt%. *Symbols* for MBOB ultramafics as in Fig. 2a. *Vertical bars* Mid Atlantic Ridge (*MAR*) peridotites (Bonatti et al. 1971; Shibata and Thompson 1986; Casey 1997). *Horizontal bars* East Pacific Rise (*EPR*) peridotites (Constantin 1995; Niu and Hékinian 1997). *Down white triangles* Oman ophiolite peridotites (Godard et al. 2000). *Crosses* Supra-subduction zone peridotites (Parkinson and Pearce 1998; Pearce et al. 2000)
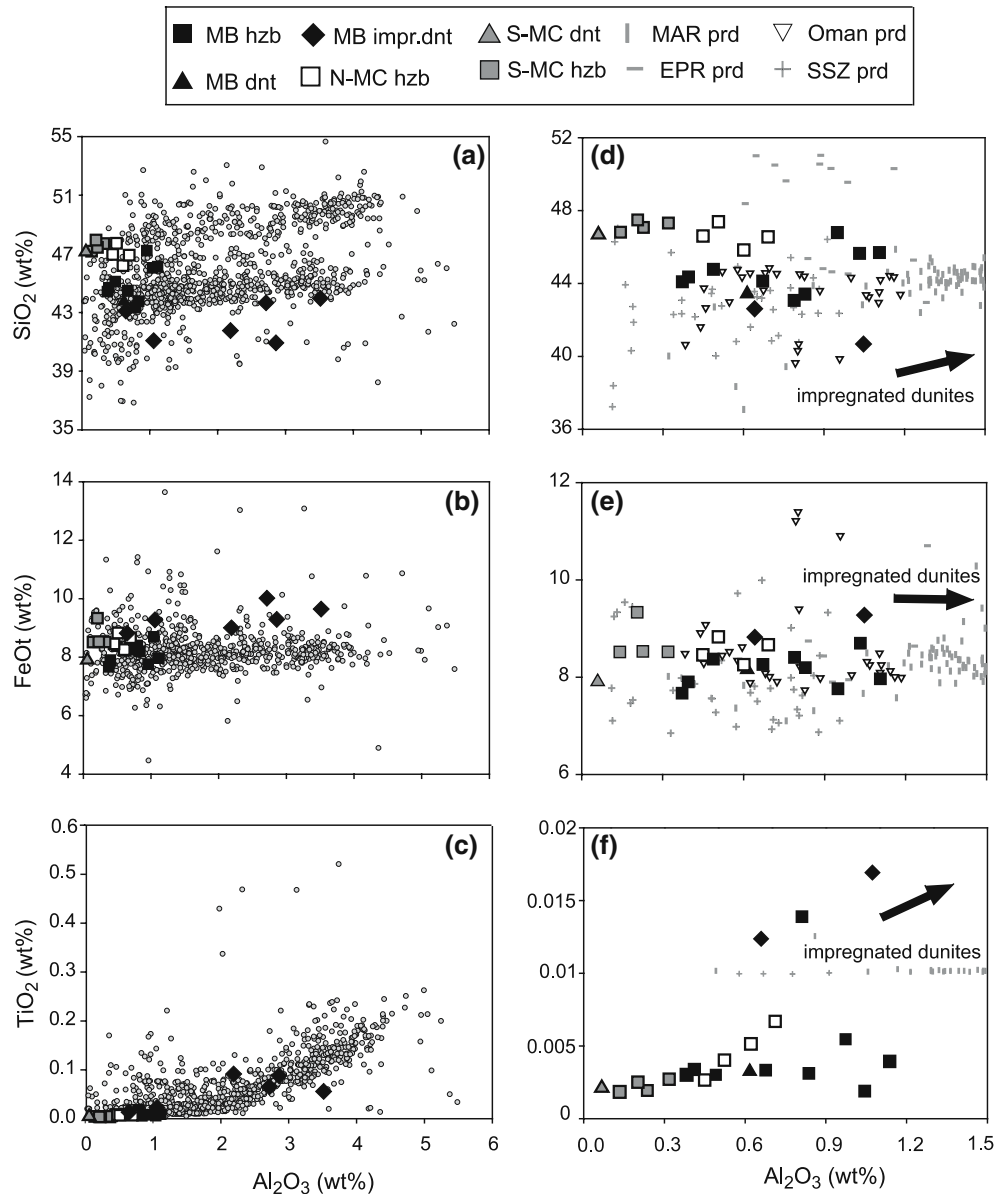
variable positive Eu anomalies, and generally flat HREE segments (Fig. 9b, c). One exception to this general trend is represented by the slight negative anomaly in Eu exhibited by the amphibole-rich dyke from Mayarí-Cristal massif (Fig. 9d).

Figure 10 shows the distribution of lithophile trace elements normalized to primitive mantle for the MBOB sills, dykes and layered gabbros. All samples, except of the amphibole-bearing dyke from Mayarí-Cristal massif, exhibit a positive Sr spike. Moa-Baracoa layered gabbros display quite homogeneous patterns. They are characterized by positive spikes for Rb and regular enrichment from Th to Sr; the gabbros from the lower region of the crustal section differ from the others for lower contents in Rb. Moa-Baracoa sill patterns are relatively depleted in Th and Zr and show a steady enrichment towards the more compatible elements.

MBOB dykes display flat patterns, characterized by positive anomalies in Cs and relative depletion in Th, U and Nb; only the amphibole-bearing dyke from Mayarí-Cristal massif differs from this trend.

Discussion

Origin of the highly depleted signature and low bulk MgO/SiO₂ ratio in MBOB peridotites

Mayarí-Baracoa Ophiolitic Belt harzburgites exhibit a highly depleted signature in terms of their modal compositions and whole rock contents in major and incompatible trace elements, suggesting that they are residues after high extents of partial melting. The highly residual character of MBOB harzburgites is attested by:
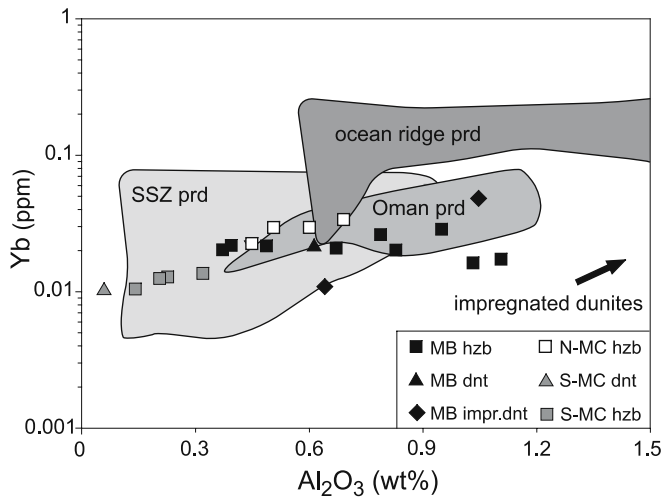
Fig. 5 Yb (ppm) versus Al_2O_3 (anhydrous wt%) whole rock contents of Mayarí-Baracoa peridotites. Published data are displayed for comparison: supra-subduction zone (*SSZ*) peridotite field from Parkinson and Pearce (1998) and Pearce et al. (2000); Oman ophiolite peridotite field from Godard et al. (2000); ocean ridge peridotite field from Bonatti et al. (1971), Shibata and Thompson (1986), Casey (1997), Constantin (1995), Niu and Hékinian (1997). *Symbols* for MBOB ultramafics as in Fig. 2a

(1) their lack of primary cpx or its alteration relics (Fig. 2a); (2) their very low whole rock Al_2O_3 ($0.14 < Al_2O_3$ anhydrous wt% < 1.11) and HREE ($0.06 < Yb_C < 0.2$) contents which are only comparable to those of supra-subduction and highly depleted ophiolitic and ocean ridge peridotites (Fig. 5); and (3) their very low contents in lithophile trace elements which are well below primitive mantle values (Fig. 7). This refractory character has been confirmed by Gervilla et al. (2005), who demonstrate that the Os isotopic signature of MBOB chromitite indicates a highly depleted mantle source.

Figure 11 shows the V versus Yb diagram for MBOB peridotites. V and Yb are reputed virtually immobile during alteration processes (Niu 2004) and they have been successfully used as proxies to infer the prevailing conditions of oxygen fugacity and the degree of partial melting in mantle peridotites (Pearce et al. 2000; Lee et al. 2003; Canil 2004 and references therein). When compared to the curves calculated for near-fractional melting of spinel peridotite at different conditions of oxygen fugacity (Pearce et al. 2000), the compositions of MBOB peridotites are consistent with 20–30% near-fractional melting at fO_2 varying between $-1 < QFM < 1$ (Fig. 11). This not only confirms the highly residual nature of MBOB peridotites, but also suggests that fO_2 conditions prevailing during melting are similar to those of both ocean ridge and Izu-Bonin-Mariana forearc peridotites (cf. Fig. 1 of Lee et al. 2003). We remark that the composition of southern Mayarí-Cristal peridotites (dark-grey symbols in Fig. 11) is consistent with higher extents of melt extraction ($> 25\%$) and slightly higher average fO_2 than other MBOB peridotites.
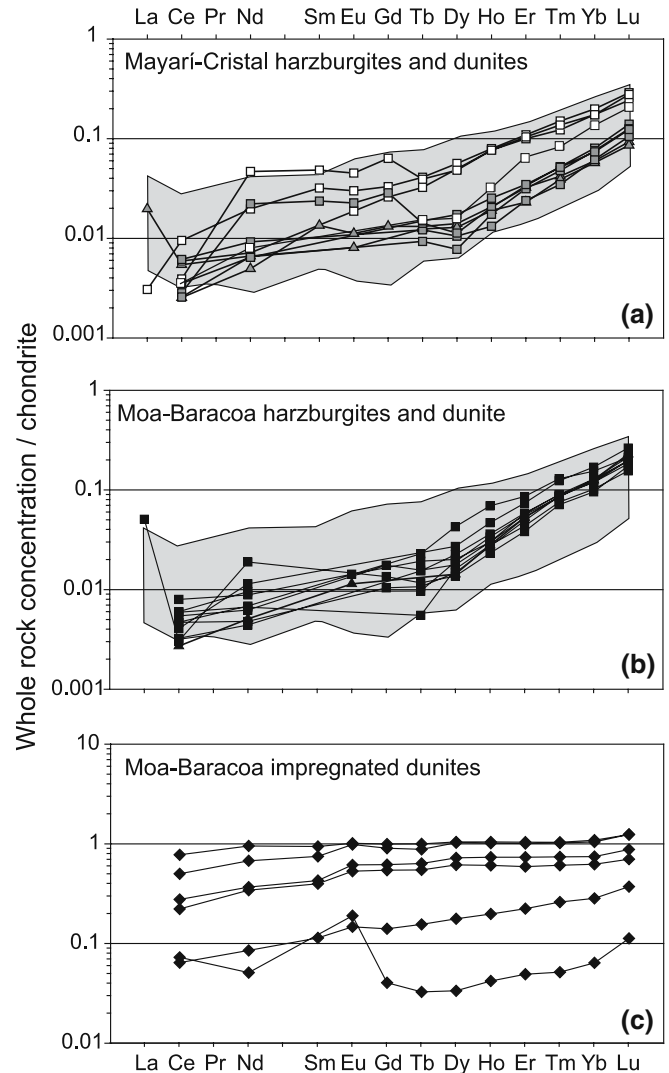
Fig. 6 Chondrite-normalized abundances of REE in Mayarí-Baracoa peridotites (whole rock analyses). *Symbols* as in Fig. 2a. Normalizing values from Sun and McDonough (1989). *Shaded area* in **a** and **b** encloses composition range of supra-subduction zone peridotites from Izu-Bonin-Mariana forearc (Parkinson and Pearce 1998)

Except for impregnated dunites, most MBOB peridotites plot below the terrestrial mantle array (Jagoutz et al. 1979; Hart and Zindler 1986) in the MgO/SiO_2 versus Al_2O_3/SiO_2 diagram (Fig. 12a). This departure from the mantle array trend is specially marked for Mayarí-Cristal peridotites that display the lowest MgO/SiO_2 ratios. Thus, for most MBOB harzburgites different partial melting scenarios fail to explain their low MgO/SiO_2 ratio (Fig. 12a) and their unusually high SiO_2 and FeOt contents for a given Al_2O_3/SiO_2 ratio (Fig. 12b, c). Low MgO/SiO_2 ratios in such altered peridotites may be caused by MgO loss during seafloor weathering (Snow and Dick 1995; Niu 2004). Assuming that the primary MgO/SiO_2 ratios laid on the mantle array and the Al_2O_3/SiO_2 ratios have not been perturbed by alteration (cf. Snow and Dick 1995; Niu 2004), we can estimate the MgO loss underwent by MBOB

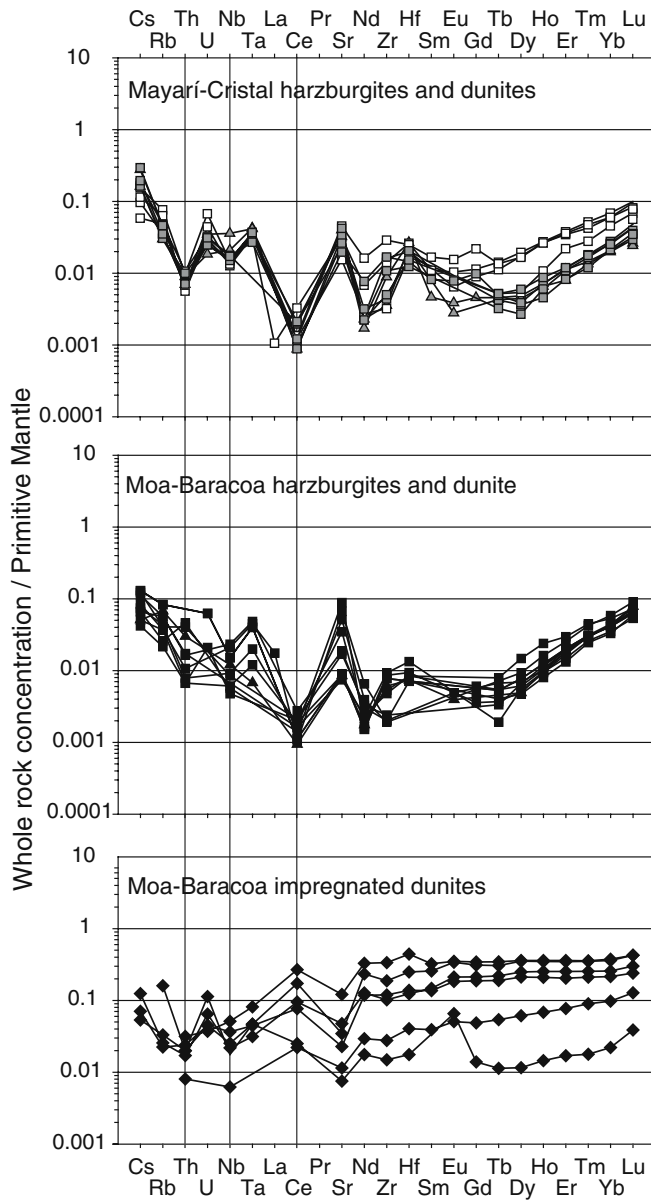peridotites. The difference between recalculated (open symbols in Fig. 12) and actual compositions (dark-grey symbols) implies relative MgO loss of about 6 wt% on average, which is consistent with previous Mg-loss estimates for highly altered abyssal peridotites (Niu 2004). Unlike actual values, the recalculated compositions of MBOB peridotites have SiO_2 contents that are consistent with a high extent of partial melting at low to moderate pressures (Fig. 12b). However, the recalculated compositions have unusually high FeOt contents to be residues of partial melting. Ocean ridge peridotites also display higher FeOt contents than those predicted by partial melting models (Niu 1997; Asimow 1999), and these variations are usually interpreted as due to ol addition after melting (Niu 1997). Alternatively, Herzberg
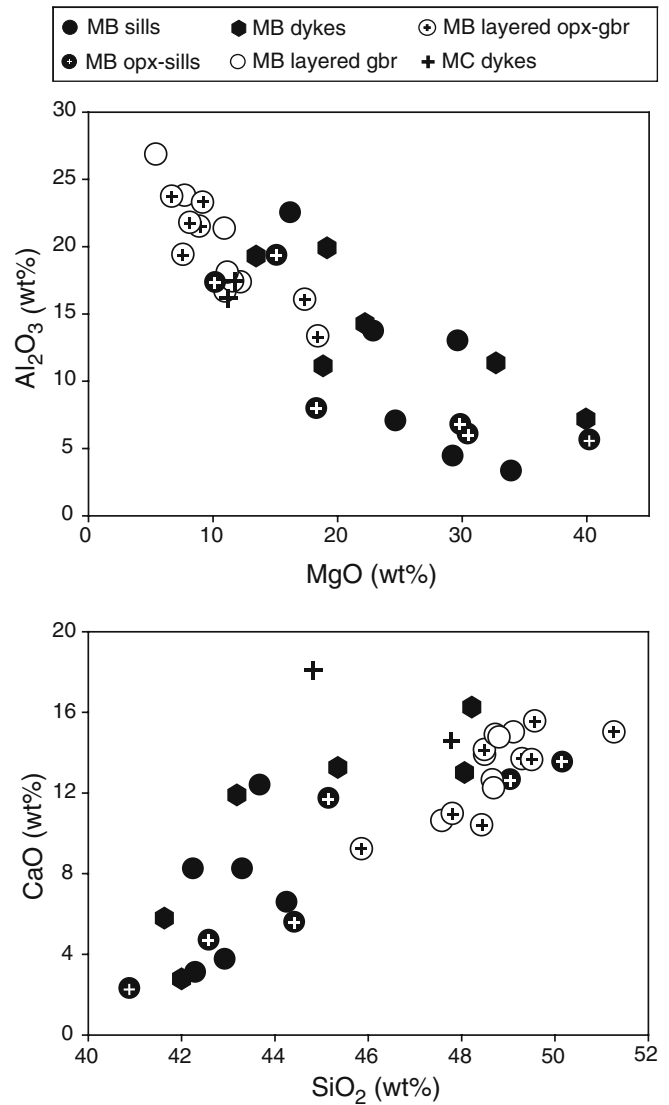
Fig. 8 Whole rock major element compositions of Mayarí-Baracoa sills, dykes and layered gabbros illustrated by Al_2O_3 vs. MgO and CaO vs. SiO_2. All data on anhydrous basis in wt%. *Symbols* as in Fig. 2b

(2004) states that high FeOt and low MgO/SiO_2 ratios are characteristic of supra-subduction peridotites.

We hence conclude that, even if primary SiO_2 enrichment (e.g. Kelemen et al. 1992, 1998; Walter 2003 and references therein) cannot be fully ruled out for two southern Mayarí-Cristal harzburgites that show rather high abundances in modal opx (Fig. 2a), the good concordance between the recalculated compositions and the predictions of melting models supports that MBOB peridotites are highly depleted mantle rocks that lost MgO as a consequence of seafloor weathering.

Evidences of melt/rock interaction in MBOB peridotites

As attested by modal compositions and major element contents, the overall low amount of lithophile trace
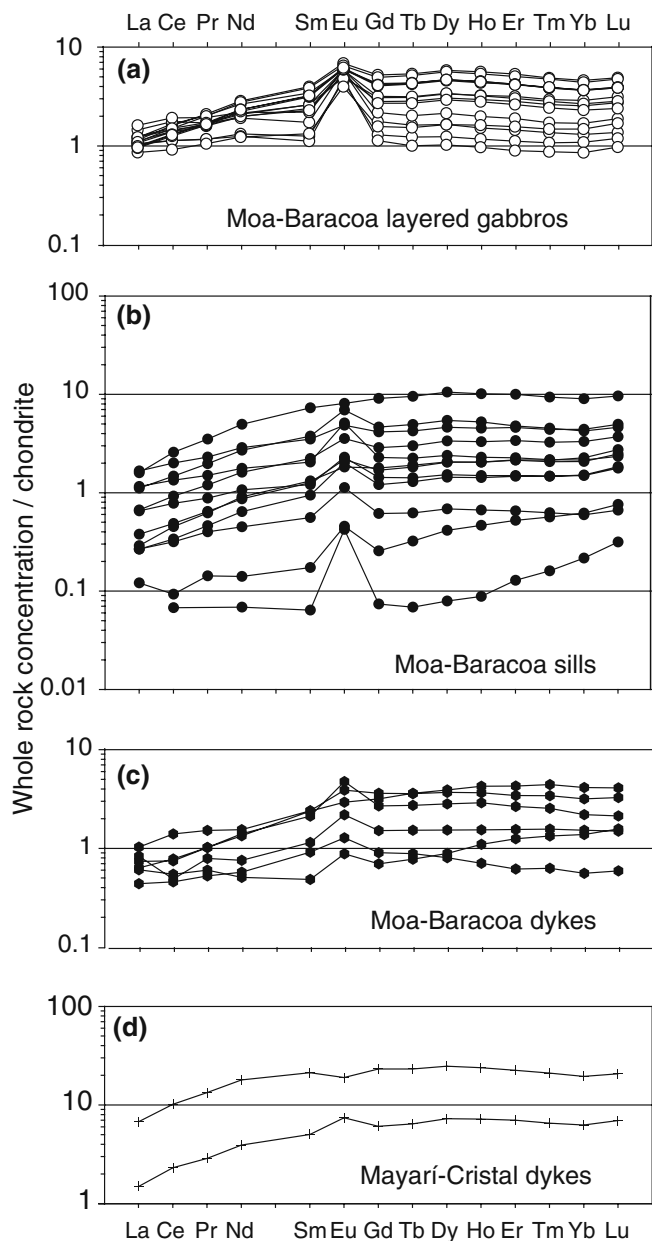
Fig. 9 Chondrite-normalized REE patterns of Mayarí-Baracoa sills, dykes and layered gabbros (whole rock analyses). *Symbols* as in Fig. 2b. Normalizing values from Sun and McDonough (1989)
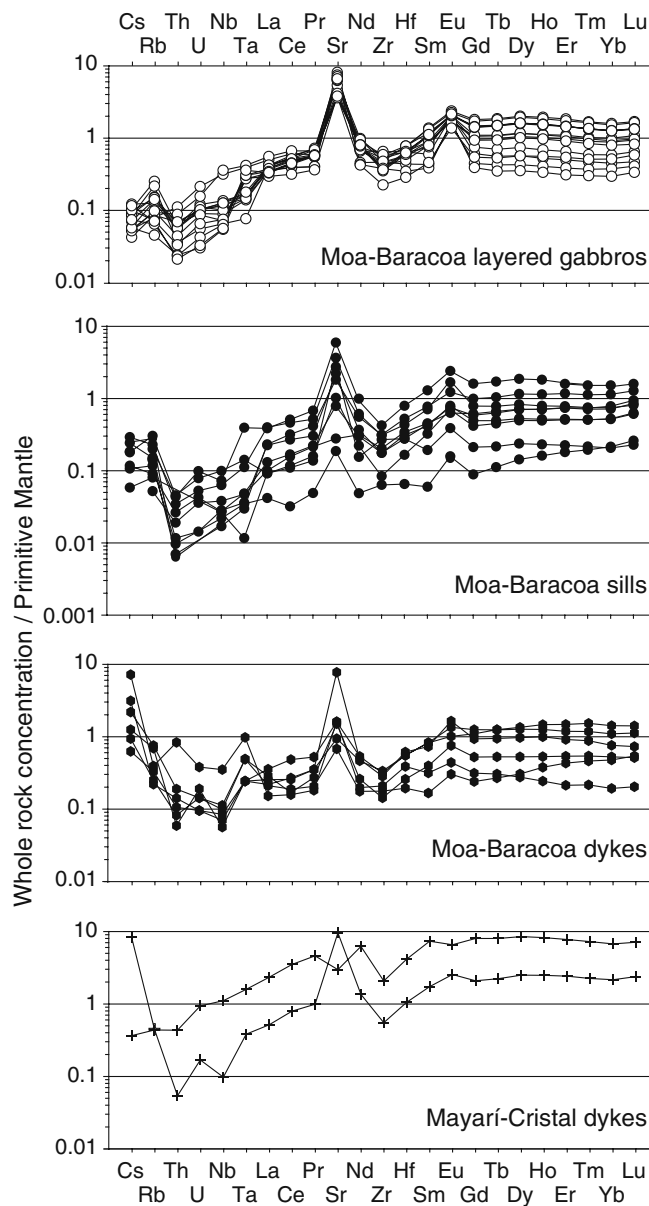

Fig. 10 Primitive mantle-normalized trace element patterns of Mayarí-Baracoa sills, dykes and layered gabbros (whole rock analyses). *Symbols* as in Fig. 2b. Normalizing values from Sun and McDonough (1989)

elements is consistent with the highly residual character of MBOB peridotites. Nevertheless, their U-shaped Primitive Mantle normalized patterns (Fig. 7) display low LREE/HREE fractionation and variable enrichment in Nb and Ta relative to neighbouring elements indicating that these peridotites are not simply partial melting residues.

Enrichment in most incompatible trace elements is usually observed in oceanic and subcontinental peridotites (e.g. Bodinier and Godard 2003 and references therein) and may be due to alteration or primary mantle processes. However, it is unlikely that LREE are mobilized by fluids during serpentinization and seafloor

weathering as they show positive correlation with immobile HFSE in highly altered abyssal peridotites (Niu 2004). Moreover, highly incompatible trace elements commonly reputed immobile (Th, Nb and Ta) also exhibit relative enrichment in MBOB peridotites. This cannot be ascribed to secondary remobilization but is most likely due to mantle processes.

Mayarí-Baracoa Ophiolitic Belt peridotites display REE patterns similar to Oman (Godard et al. 2000) and Izu-Bonin-Mariana peridotites (Parkinson and Pearce 1998), both interpreted as portions of lithospheric mantle re-equilibrated with percolating melts during melt transport by reactive porous flow (e.g. Navon and
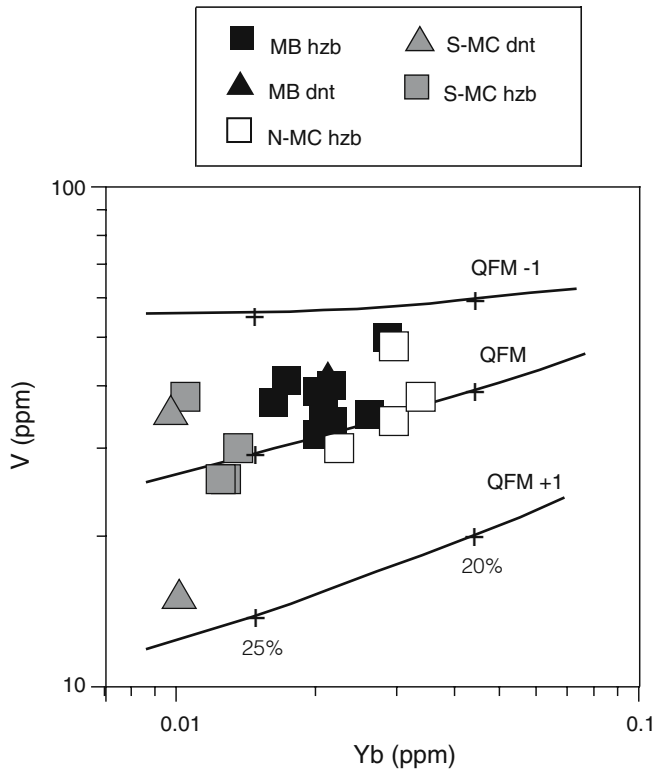
Fig. 11 V–Yb (ppm) whole rock contents of Mayarí-Baracoa mantle peridotites. Modelling of melting extraction and oxygen fugacities from Pearce et al. (2000), and references therein. fO_2 expressed as log-unit deviations from QFM; *QFM* quartz–fayalite–magnetite buffer. *Symbols* as in Fig. 2a

Stolper 1987; Bodinier et al. 1990; Vernières et al. 1997). Additionally, in MBOB peridotites Nb and Ta are generally enriched relative to Th and LREE (average $(Nb/Th)_{PM} = 1.7$; $(Nb/Ce)_{PM} = 10.5$) conversely to what is observed in oceanic abyssal peridotites (Niu 2004). This characteristic has already been remarked for MBOB peridotites as well as for Oman and Ronda peridotites (Bodinier and Godard 2003 and references therein). Selective enrichment in Nb and Ta may be related to chromatographic interaction between migrating melts and mantle peridotite (Kelemen et al. 1993) or to precipitation of Nb-rich rutile from volatile-rich magmas (Bodinier et al. 1996; Garrido et al. 2000) that may lead to corresponding depletion of Nb and Ta in ascending melts as peculiar to arc lavas.

Genetical relationships between gabbroic cumulates and volcanic rocks

The Mg# content of ol ($\leq$ 82) in MBOB gabbros and the strong positive Eu (and Sr) anomalies of their normalized patterns indicate that they are cumulitic rocks crystallized from mantle-derived basaltic melts. A similar origin has been proposed for the MTZ gabbro sills and lower crustal gabbros in the Oman ophiolite (Pallister and Knight 1981; Kelemen et al. 1997; Korenaga and Kelemen 1997) and many other ophiolites.
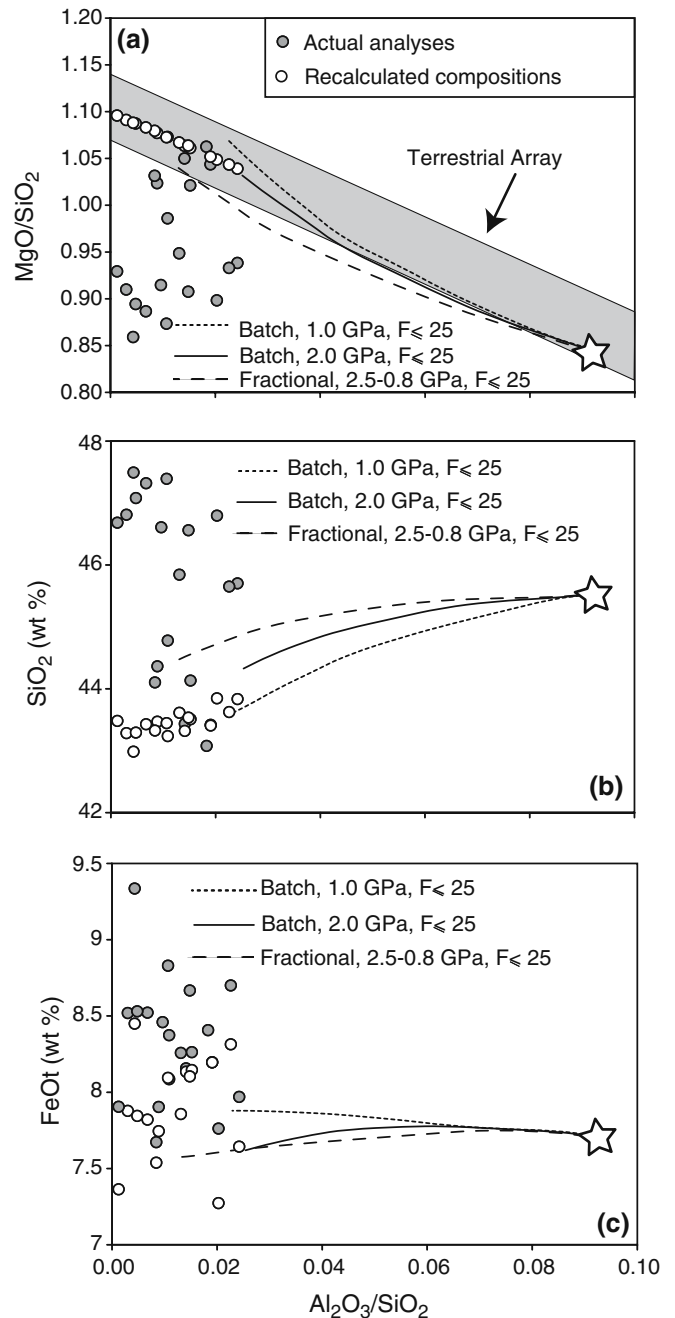
Fig. 12 Comparison between actual bulk-rock analyses (*dark-grey circles*) and recalculated bulk rock compositions after MgO addition (*open circles*) for MBOB peridotites on Al_2O_3/SiO_2 vs. MgO/SiO_2 (a), SiO_2 (b), FeOt (c). All data on anhydrous basis in wt%. Terrestrial array in **a** from Jagoutz et al. (1979) and Hart and Zindler (1986). Curves of polybaric near-fractional and isobaric batch melting of fertile mantle source (*star*) redrawn from Niu (1997)

The amphibole-rich Mayarí-Cristal dyke is an exception, as its pattern and high content of REE are consistent with a composition closer to that of aggregated melt.

Because of the lack of clear intrusive relationships owing to pervasive deformation, a critical issue for the regional geology of the MBOB is the genetic relationship

between gabbroic rocks and spatially-related lavas. The Quibiján volcanics are in tectonic contact with the ophiolitic section of the Moa-Baracoa massif and they mainly consist of basalts interbedded with cherts, hyaloclastites, and minor tuffaceous rocks. The only available geochemical data on this volcanic formation are those of Kerr et al. (1999) and Proenza et al. (2006) for two pillow basalts from the locality of Morel, which have been interpreted as back-arc basalts. The Téneme volcanic formation is in tectonic contact with Mayarí-Cristal ophiolitic rocks. These volcanics are mainly constituted by basalts and basaltic andesites and they have been interpreted as island arc tholeiites (Proenza et al. 2006).

The calculated Mg# average value for liquids in equilibrium with the ol of Moa-Baracoa cumulates is 0.51 (FeO/MgO ol–liquid K_d from Roeder and Emslie 1970); such a low value implies that the parental magma experienced intense crystal fractionation after a primary mantle derived melt. The REE equilibrium concentrations in the melts coexisting with the cumulate gabbros have been calculated following the method of Bédard (1994). The REE patterns of the melts in trace element exchange equilibrium with MBOB gabbroic rocks show an N-MORB pattern (Fig. 13) with $(La/Yb)_C$ and $(Ce/Sm)_C$ ratios ranging between 0.5–0.9 and 0.6–1.0, respectively. For two crustal gabbros from the Moa-Baracoa massif, we have performed additional in situ analyses of the trace element content of cpx by LA-ICP-MS (Table 4) (Fig. 13c). The melts in equilibrium with cpx have been calculated using K_d cpx/melt reported by Hart and Dunn (1993). The calculated melts using this alternative procedure are identical to those obtained by whole rock and modal data, confirming that gabbros from the Moa-Baracoa crustal section were in trace element equilibrium with N-MORB magmas (Fig. 13c).

In Fig. 13a, b we compare the REE patterns of liquids in equilibrium with Mayarí-Cristal and Moa-Baracoa cumulates with the REE patterns of Téneme and Morel volcanics, respectively. Téneme volcanics exhibit patterns enriched in LREE and flat to slightly depleted for MREE and HREE which are very different from the liquid in equilibrium with the Mayarí-Cristal cumulate dyke. On the other hand, Morel volcanics display N-MORB type REE patterns comparable with calculated melts in equilibrium with Moa-Baracoa gabbros. Furthermore, the average Mg# of Morel lavas matches those in equilibrium with ol of Moa-Baracoa cumulates. These results indicate that Morel volcanics are melts derived after crystallization of the gabbro section of the Moa Baracoa massif. Conversely, the limited available data indicate that Mayarí-Cristal dykes and Téneme volcanics are not cogenetic. However, radiogenic isotopic and geochronological data are needed to clarify the petrogenetical relationships between Mayarí-Cristal ophiolitic massif and Téneme volcanics.
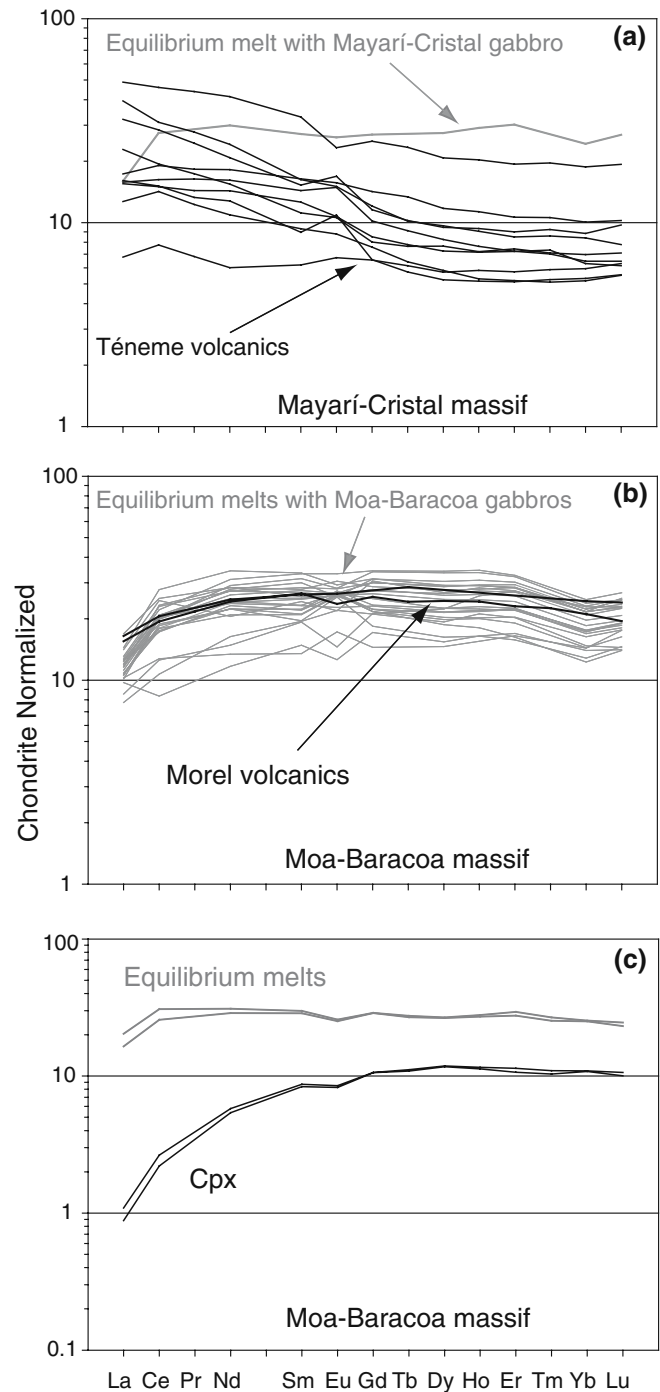

Fig. 13 Calculated REE patterns of liquids in equilibrium with Mayarí-Baracoa cumulate gabbros compared to Téneme and Morel volcanics. a Grey line represents the calculated REE pattern of the liquid coexisting with Mayarí-Cristal cumulate dyke. This pattern is compared to REE contents of Téneme volcanics (black lines) (Proenza et al. 2006). b Grey lines are REE patterns of liquids in equilibrium with Moa-Baracoa sills, dykes and layered cumulate gabbros. Patterns of limited available data on volcanics from the locality of Morel (Kerr et al. 1999; Proenza et al. 2006) are shown for comparison (black lines). c Black lines are average REE patterns of cpx for two layered gabbros from Moa-Baracoa massif. Grey lines are calculated patterns for liquids in equilibrium with cpx

Tectonic setting of Moa-Baracoa and Mayarí-Cristal massifs

The Moa-Baracoa and Mayarí-Cristal peridotites have mineral and whole-rock compositions characteristic of mantle sections from both ocean basins and supra-subduction settings. In this way they are similar to Conical Seamount peridotites from the Izu-Bonin-Mariana forearc and to the South Sandwich forearc peridotites interpreted as residual mid-ocean ridge or back-arc mantle accreted on the forearc mantle lithosphere (Parkinson and Pearce 1998; Pearce et al. 2000).

We note that the oxygen fugacities displayed by MBOB melting residues (Fig. 11) are toward the upper end of the ocean ridge range ($-3 < QFM < 0$ according to Lee et al. 2003) which may support a back-arc setting with a slight supra-subduction zone signature for the MBOB ridge. For the Mayarí-Cristal massif an ancient supra-subduction setting is corroborated by the spinel mineral chemistry of dunites that indicates they formed when subduction-related magmas interacted with mantle tectonites (Fig. 3d).

The mafic rocks of the MBOB display MORB-like or transitional MORB-IAT geochemical signatures (Figs. 9, 10) consistent with an origin at a mid-ocean ridge or back-arc spreading centre. This last interpretation is supported by the genetical link between Moa-Baracoa cumulates and spatially-related back-arc volcanics (Fig. 13b).

We stress that Moa-Baracoa and Mayarí-Cristal massifs significantly differ in terms of field occurrence, mineral chemistry and geochemical characteristics. (1) The Moa-Baracoa massif shows a continuous plutonic section with a well-defined Moho transition zone, whereas both are absent in the Mayarí-Cristal massif. Moreover, (2) the Mayarí-Cristal massif shows higher ol Mg# and spinel Cr# in peridotites (Fig. 3a, b), (3) higher An content in plagioclase from mafic rocks (Fig. 3c) and (4) a more depleted nature and slightly higher values of fO_2 in melting residues (Fig. 11). We interpret these differences as evidence that the two massifs were not part of a single lithospheric section, but that the Mayarí-Cristal massif was a portion of lithosphere located closer to the paleo-arc than the Moa-Baracoa massif, as attested by a more important role of H_2O in its petrogenesis.

The inferred conclusions are consistent with the model of Iturralde-Vinent (1994) who provided evidences that MBOB is a portion of an original back-arc lithosphere. In this context, we propose a relatively close arc position for the original setting of the Mayarí-Cristal massif based on the stronger imprint of a subduction-related geochemical signature indicating the increasing influence of slab melts or fluids. The Mayarí-Cristal transitional (MORB-IAT) lithosphere may have been finally accreted on forearc terranes where subduction-related magmas interacted with pre-existing mantle lithosphere (Proenza et al. 1999b).

Conclusions

Based upon the presented data about field relationships, petrography, mineral chemistry, and whole rock compositions of the Moa-Baracoa and Mayarí-Cristal ophiolitic massifs we infer the following:

1. Moa-Baracoa and Mayarí-Cristal massifs are two ophiolitic complexes made up of harzburgite tectonites and minor sub-concordant dunites cut by gabbroic dykes. In terms of field occurrence the two massifs differ strikingly: Moa-Baracoa displays a well developed Moho transition zone and plutonic crustal section whereas both are absent in the Mayarí-Cristal massif.
2. Modal abundances, major and trace element whole rock compositions of Moa-Baracoa and Mayarí-Cristal harzburgites indicate that they are residues of high extents (20–30%) of partial melting under intermediate fO_2 conditions ($-1 < QFM < 1$); the Mayarí-Cristal southern harzburgites record the highest melting degrees. Low MgO/SiO_2 whole rock ratios in peridotites are caused by relative MgO loss of 6 wt% on average due to intense seafloor weathering.
3. Peridotites extensively interacted by reactive porous flow with percolating melts leading to selective enrichment of Th, Nb, Ta and LREE in refractory melting residues.
4. The calculated REE patterns and Mg# of melts in trace-element exchange equilibrium with Moa-Baracoa cumulate gabbros show that they were cogenetic with Morel back-arc volcanics. Conversely, the Mayarí-Cristal gabbro dyke is not in equilibrium with the spatially-related arc volcanics of the Téneme Formation.
5. We propose that the Moa-Baracoa and Mayarí-Cristal massifs represent two portions of back-arc lithosphere. Moa-Baracoa massif displays MOR-like signature and melting oxygen fugacities consistent with an original position located close to the back-arc spreading centre. Mayarí-Cristal lithosphere exhibits an increasing role of H_2O in its petrogenesis and evidences of interaction with subduction-related (IAT) magmas, attesting for an original setting located closer to the paleo-volcanic arc than Moa-Baracoa.

References

Asimow PD (1999) A model that reconciles major- and trace-element data from abyssal peridotites. Earth Planet Sci Lett 169:303–319

Baker MB, Beckett JR (1998) The origin of abyssal peridotites: a reinterpretation of constraints based on primary bulk compositions. Earth Planet Sci Lett 171:49–61

Beard JS (1986) Characteristic mineralogy of arc-related cumulate gabbros: implications for the tectonic setting of gabbroic plutons and for andesite genesis. Geology 14(10):848–851

Bédard JH (1994) A procedure for calculating the equilibrium distribution of trace elements among the minerals of cumulate rocks, and the concentration of trace elements in the coexisting liquids. Chem Geol 118(1–4):143–153

Bodinier JL, Godard M (2003) Orogenic, ophiolitic, and abyssal peridotites. In: Carlson RW (ed) Treatise on geochemistry. The mantle and core, vol 2. Elsevier, Amsterdam, pp 103–170

Bodinier JL, Vasseur G, Vernières J, Dupuy C, Fabries J (1990) Mechanisms of mantle metasomatism—geochemical evidence from the Lherz orogenic peridotite. J Petrol 31(3):597–628

Bodinier JL, Merlet C, Bedini RM, Simien F, Remaidi M, Garrido CJ (1996) Distribution of niobium, tantalum, and other highly incompatible trace elements in the lithospheric mantle: the spinel paradox. Geochim Cosmochim Acta 60(3):545–550

Bonatti E, Honnorez J, Ferrara G (1971) Peridotite-gabbro-basalt complex from the equatorial mid-Atlantic ridge. Philos Trans R Soc A268:385–402

Canil D (2004) Mildly incompatible elements in peridotites and the origins of mantle lithosphere. Lithos 77:375–393

Cannat M, Lagabrielle Y, Bougault H, Casey J, deCoutures N, Dmitriev L, Fouquet Y (1997) Ultramafic and gabbroic exposures at the Mid-Atlantic Ridge: geological mapping in the 15 degrees N region. Tectonophysics 279(1–4):193–213

Casey JF (1997) Comparison of major and trace element geochemistry of abyssal peridotites and mafic plutonic rocks with basalt from the MARK region of the mid-Atlantic ridge. In: Karson JA, Cannat M, Miller DJ, Elthon D (eds) Mid-Atlantic ridge: leg 153, sites 920–924, vol 153. College Station, pp 181–241

Cazañas X, Proenza J, Kysar Mattietti G, Lewis J, Melgarejo JC (1998) Rocas volcánicas de las series Inferior y Media del Grupo El Cobre en la Sierra Maestra (Cuba Oriental): volcanismo generado en un arco de islas tholeiítico. Acta Geol Hispan 33:277–333

Cobiella-Reguera JL (2002) Remains of oceanic lithosphere in Cuba. Types, origins and emplacement ages. In: Jackson T (ed) Caribbean geology into the third millennium. Transactions of the fifteenth Caribbean geological conference. University of the West Indies, pp 35–46

Constantin M (1995) Petrologie des gabbros et peridotites de la dorsale Est-Pacifique: la transition croute-manteau aux dorsales rapides. In: Geologie Bretagne Occidentale, Brest, p 286

Dick HJB (1989) Abyssal peridotites, very slow spreading ridges and ocean ridge magmatism. In: Saunders AD, Norry MJ (eds) Magmatism in the Ocean Basins, vol 42. Geological Society Special Publication, pp 71–105

Dick HJB, Fisher RL, Bryan WB (1984) Mineralogic variability of the uppermost mantle along mid-ocean ridges. Earth Planet Sci Lett 69(1):88–106

García-Casco A, Pérez de Arce C, Millán G, Iturralde-Vinent MA, Fonseca E, Torres-Roldán R, Núñez K, Morata D (2003) Metabasites from the Northern serpentinite belt (Cuba) and a metamorphic perspective of the plate tectonic models for the Caribbean region. In: Field workshop of the IGCP Project 433 Scientific Meeting, V Geological and Mining Congress of the Cuban Geological Society

Garrido CJ, Bodinier JL, Alard O (2000) Incompatible trace element partitioning and residence in anhydrous spinel peridotites and websterites from the Ronda orogenic peridotite. Earth Planet Sci Lett 181(3):341–358

Gervilla F, Proenza JA, Frei R, González-Jiménez JM, Garrido CJ, Melgarejo JC, Meibom A, Díaz-Martinez R, Lavaut W (2005) Distribution of platinum-group elements and Os isotopes in chromite ores from Mayarí-Baracoa Ophiolitic Belt (eastern Cuba). Contrib Mineral Petrol 150:589–607

Godard M, Jousselin D, Bodinier JL (2000) Relationships between geochemistry and structure beneath a palaeo-spreading centre: a study of the mantle section in the Oman ophiolite. Earth Planet Sci Lett 180(1–2):133–148

Govindaraju K (1994) Compilation of working values and sample description for 383 geostandards. Geostand Newslett XVIII (Spec. Issue)

Hart SR, Dunn T (1993) Experimental cpx/melt partitioning of 24 trace elements. Contrib Mineral Petrol 113:1–8

Hart SR, Zindler A (1986) In search of a bulk-Earth composition. Chem Geol 57:247–267

Hellebrand E, Snow JE, Hoppe P, Hofmann AW (2002) Garnet-field melting and late-stage refertilization in 'residual' abyssal peridotites from the Central Indian Ridge. J Petrol 43(12):2305–2338

Herzberg C (2004) Geodynamic information in peridotite petrology. J Petrol 45:2507–2530

Ionov DA, Savoyant L, Dupuy C (1992) Application of the ICP-MS technique to trace-element analysis of peridotites and their minerals. Geostand Newslett 16(2):311–315

Iturralde-Vinent MA (1994) Cuban geology: a new plate tectonic synthesis. J Petrol Geol 17:39–69

Iturralde-Vinent MA (1996) Introduction to cuban geology and geophysics. In: Iturralde-Vinent MA (ed) Ofiolitas y Arcos Volcanicos de Cuba. IUGS-UNESCO Project 364. Caribbean Ophiolites and Volcanic Arcs. Special Contribution, Miami, pp 3–35

Iturralde-Vinent MA (1998) Sinopsis de la Constitución Geológica de Cuba. In: Melgarejo JC, Proenza JA (eds) Geología y Metalogenia de Cuba: una introducción. Acta Geologica Hispanica, vol 33(1–4), pp 9–56

Iturralde-Vinent MA (2003) The relationship between the ophiolites, the metamorphic terrains, the Cretaceous volcanic arcs and the Paleocene–Eocene volcanic arc. Field guide to a geological excursion to Eastern Cuba. In: V Cuban Geological and Mining Congress, March 2003. IGCP Project 433. Cuban Geological Society, p 16

Iturralde-Vinent MA, Díaz-Otero C, Rodríguez-Vega A, Díaz-Martínez R (2006) Tectonic implications of paleontologic dating of Cretaceous sections of northeastern Cuba. Geol Acta (in press)

Jagoutz E, Palme H, Blum H, Cendales M, Dreibus G, Spettel B, Lorenz V, Wanke H (1979) The abundances of major, minor and trace elements in the Earth's mantle as derived from primitive ultramafic nodules. Proceeding of 10th lunar planetary science conference. Geochim Cosmochim Acta Suppl 10:2031–2051

Jochum KP, Seufert HM, Thirwall MF (1990) Muti-element analysis of 15 international standard rocks by isotope-dilution spark source mass spectrometry (ID-SSMS). Anal Chem 331:104–110

Jousselin D, Nicolas A (2000) The Moho transition zone in the Oman ophiolite: relation with wehrlites in the crust and dunites in the mantle. Mar Geophys Res 21(3–4):229–241

Kelemen PB, Dick HJB, Quick JE (1992) Formation of harzburgite by pervasive melt rock reaction in the upper mantle. Nature 358(6388):635–641

Kelemen PB, Shimizu N, Dunn T (1993) Relative depletion of niobium in some arc magmas and the continental crust: partitioning of K, Nb, La and Ce during melt/rock reaction in the upper mantle. Earth Planet Sci Lett 120:111–134

Kelemen PB, Koga K, Shimizu N (1997) Geochemistry of gabbro sills in the crust-mantle transition zone of the Oman ophiolite: implications for the origin of the oceanic lower crust. Earth Planet Sci Lett 146(3–4):475–488

Kelemen PB, Hart SR, Bernstein S (1998) Silica enrichment in the continental upper mantle via melt/rock reaction. Earth Planet Sci Lett 164(1–2):387–406

Kerr AC, Iturralde-Vinent MA, Saunders AD, Babbs TL, Tarney J (1999) A new plate tectonic model of the Caribbean: implications from a geochemical reconnaissance of Cuban Mesozoic volcanic rocks. Geol Soc Am Bull 111(11):1581–1599

Koga KT, Kelemen PB, Shimizu N (2001) Petrogenesis of the crust–mantle transition zone and the origin of lower crustal wehrlite in the Oman ophiolite. Geochem Geophys Geosyst 2:art. no. 2000GC000132

Korenaga J, Kelemen PB (1997) Origin of gabbro sills in the Moho transition zone of the Oman ophiolite: implications for magma transport in the oceanic lower crust. J Geophys Res Solid Earth 102(B12):27729–27749

Kysar Mattietti G (2001) The role of Paleogene magmatism in the evolution of the northern Caribbean margin. In: The Sierra Maestra (southern Cuba). George Washington University, p 187

Lee C-TA, Brandon AD, Norman M (2003) Vanadium in peridotites as a proxy of paleo-fO$_2$ during partial melting: prospects, limitations and implications. Geochim Cosmochim Acta 67(16):3045–3064

Meschede M, Frisch W (1998) A plate tectonic model for the Mesozoic and Early Cenozoic history of the Caribbean plate. Tectonophysics 296:269–291

Metzger EP, Miller RB, Harper GD (2002) Geochemistry and tectonic setting of the ophiolitic ingalls complex, North Cascades, Washington: implications for correlations of Jurassic cordilleran ophiolites. J Geol 110:543–560

Navon O, Stolper E (1987) Geochemical consequences of melt percolation: the upper mantle as a chromatographic column. J Geol 95:285–307

Nicolas A (1989) Structures of ophiolites and dynamics of oceanic lithosphere. Kluwer, Dordrecht, p 367

Niu Y (1997) Mantle melting and melt extraction processes beneath ocean ridges: evidence from abyssal peridotites. J Petrol 38:1047–1074

Niu Y (2004) Bulk-rock major and trace element compositions of abyssal peridotites: implications for mantle melting, melt extraction and post-melting processes beneath mid-ocean ridges. J Petrol 45:2423–2458

Niu Y, Hékinian R (1997) Basaltic liquids and harzburgitic residues in the Garrett Transform: a case study at fast-spreading ridges. Earth Planet Sci Lett 146:243–258

Niu Y, Langmuir CH, Kinzler RJ (1997) The origin of abyssal peridotites: a new perspective. Earth Planet Sci Lett 152(1–4):251–265

Ohara Y, Stern RJ, Ishii T, Yurimoto H, Yamazaki T (2002) Peridotites from the Mariana Trough: first look at the mantle beneath an active back-arc basin. Contrib Mineral Petrol 143:1–18

Pallister JS, Knight RJ (1981) Rare-earth element geochemistry of the Samail ophiolite near Ibra, Oman. J Geophys Res 86:2673–2697

Parkinson IJ, Pearce JA (1998) Peridotites from the Izu-Bonin-Mariana Forearc (ODP Leg 125): evidence for mantle melting and melt-mantle interaction in a supra-subduction zone setting. J Petrol 39:1577–1618

Pearce JA, Barker PF, Edwards SJ, Parkinson IJ, Leat PT (2000) Geochemistry and tectonic significance of peridotites from the South Sandwich arc-basin system, South Atlantic. Contrib Mineral Petrol 139:36–53

Pindell JL (1994) Evolution of the Gulf of Mexico and the Caribbean. In: Donovan S, Jackson T (eds) Caribbean geology, an introduction. U.W.I. Publishers' Association, Kingston, pp 13–40

Pindell JL, Barrett SF (1990) Geological evolution of the Caribbean Region; a plate-tectonic perspective. In: Dengo G, Case J (eds) The geology of North America, vol H. The Caribbean Region. GSA, pp 405–432

Proenza J, Gervilla F, Melgarejo JC (1999a) La Moho Transition Zone en el Macizo Ofiolítico Moa-Baracoa: un ejemplo de interacción magma/peridotita. Rev Soc Geol España 12:309–327

Proenza J, Gervilla F, Melgarejo JC, Bodinier JL (1999b) Al- and Cr-rich chromitites from the Mayarí-Baracoa Ophiolitic Belt (Eastern Cuba): consequence of interaction between volatile-rich melts and peridotite in suprasubduction mantle. Econ Geol 94:547–566

Proenza J, Alfonso J, Melgarejo JC, Gervilla F, Tritlla J, Fallick AE (2003) D, O and C isotopes in podiform chromitites as fluid tracers for hydrothermal alteration processes of the Mayarí-Baracoa Ophiolitic Belt, eastern Cuba. J Geochem Explor 78–79:117–122

Proenza JA, Díaz-Martínez R, Marchesi C, Melgarejo JC, Gervilla F, Garrido CJ, Rodríguez-Vega A, Lozano-Santacruz R, Blanco-Moreno J (2006) Primitive island-arc volcanic rocks in Eastern Cuba: the Téneme Formation. Geol Acta (in press)

Roeder PL, Emslie RF (1970) Olivine-liquid equilibrium. Contrib Mineral Petrol 29:275–289

Shibata T, Thompson G (1986) Peridotites from the mid-Atlantic ridge at 43°N and their petrogenetic relation to abyssal tholeiites. Contrib Mineral Petrol 93:144–159

Snow JE, Dick HJB (1995) Pervasive magnesium loss by marine weathering of peridotite. Geochim Cosmochim Acta 59(20):4219–4235

Sun S-S, McDonough WF (1989) Chemical and isotopic systematics of oceanic basalts: implications for mantle composition and processes. In: Saunders AD, Norry MJ (eds) Magmatism in the Ocean Basins, vol 42. Geological Society Special Publication, pp 313–345

Vernières J, Godard M, Bodinier JL (1997) A plate model for the simulation of the trace element fractionation during partial melting and magma transport in the Earth's upper mantle. J Geophys Res 102:24771–24784

Walter MJ (2003) Melt extraction and compositional variability in mantle lithosphere. In: Carlson RW (ed) Treatise on geochemistry. The mantle and core, vol 2. Elsevier, Amsterdam, pp 363–394